WT cells. Finally, we cotransfected SUM149PT cells with constructs encoding both FBXW7 and HA-ubiquitin, and found that ubiquitination of mTOR was restored by exogenous *FBXW7* expression (Fig. 2E). Thus, ubiquitination of mTOR is largely, if not exclusively, mediated by binding to FBXW7.

As *FBXW7* and *PTEN* both affect signaling through mTOR, we examined the genetic status of both genes in a panel of 53 breast cancer cell lines (*11*). Quantitative TaqMan real-time polymerase chain reaction (PCR) assays of the number of copies of *FBXW7* and *PTEN* genes in each of the cell lines were in good concordance with data found by bacterial artificial chromosome (BAC) comparative genomic hybridization (CGH) microarray (see table S1). Most of the breast cancer cell lines that exhibited loss of a single copy of *FBXW7* (23 out of 53, Fig. 3A) did not show corresponding loss of *PTEN*. In contrast, of the 14 lines that showed loss of a single copy of *PTEN* (Fig. 3A), only one had also lost a copy of *FBXW7*, which suggested that *FBXW7* and *PTEN* show some functional redundancy in tumor development. Similar results were obtained by examination of the copy number status of genomic regions containing *FBXW7* and *PTEN* genes in three independent human primary breast cancer sets for which BAC CGH microarray data were available (*12*–*14*). From a total of 450 tumor and cell line DNA samples shown in Fig. 3, A to D, only 4 had lost a copies of the regions containing both genes, a result that is unlikely to be a consequence of random genetic alterations ($P = 4.9 \times 10^{-7}$).

We also considered the possibility that other somatic changes such as point mutations or gene-silencing events could affect the results. The *FBXW7* gene continued to be expressed in all 25 breast cancer cell lines examined (fig. S8), which indicated that no gene silencing had occurred, although very low levels were found in five cell lines [lanes 10, 13, 14, 16, and 20 (fig. S8)]. All of these lines had lost one copy of the *FBXW7* gene except one (SUM149PT, lane 16), in which a point mutation was detected (table S1). The *PTEN* gene was found to be silent in two cell lines (fig. S8, lanes 11 and 12), and both had lost one copy of the *PTEN* gene. Three mutations in *PTEN* were found (fig. S8 and table S1). Thus, gene silencing (for example, by promoter methylation) or point mutations in *FBXW7* and *PTEN* are relatively rare mechanisms of inactivation of these genes, in comparison with single-copy deletions. These data are further compatible with the identification of both genes as haplo-insufficient tumor suppressors (*3*, *15*, *16*).

Because deletion or mutation of *FBXW7* in human breast cancer cells leads to increased levels of mTOR, we tested the possibility that cells harboring these deletions may show increased sensitivity to the mTOR inhibitor rapamycin. We treated two breast cancer cell lines, SUM149PT cells (homozygous *FBXW7* mutations) and MDA-MB453 cells (wild-type *FBXW7*) with rapamycin and counted numbers of viable cells. SUM149PT cells proved to be very sensitive to this treatment [median inhibitory concentration (IC_{50}) < 200 nM], whereas MDA-MB453 cells were relatively resistant (IC_{50} > 2 μM) (Fig. 4A). In nude mouse xenografts, groups of five mice were injected with both cell lines, one on each flank, and were treated by intraperitoneal injection with rapamycin over an 11-day period. The SUM149PT cells showed a relative decrease in size followed by stable tumor growth, whereas the MDA-MB453 cells were relatively unaffected by treatment (Fig. 4B).

An additional set of 10 breast cancer cell lines was treated with rapamycin at concentrations of 200 and 400 nM. Cells with deletion or mutation of *FBXW7* (HBL100, 600MPE, SUM149PT, HCC3153, and HCC1143) or *PTEN* (HCC1937 and HCC3153) showed significant sensitivity to killing by rapamycin, although the magnitude of the effect varied (*17*) (Fig. 4C). To establish a direct link between loss of FBXW7 and rapamycin sensitivity, we down-regulated expression levels of FBXW7 using short hairpin RNA (shRNA) (*18*) in the rapamycin-resistant MDA-MB453 cells, which resulted in an increase in sensitivity to this drug [IC_{50}< 0.8 μM (Fig. 4D)].

Our findings implicate FBXW7 in an evolutionarily conserved pathway that controls regulation of mTOR protein levels. Because FBXW7 is a haploinsufficient tumor suppressor that undergoes heterozygous loss in a substantial proportion of human tumors, the data suggest new approaches to reduce mTOR levels in cancers by the use of drugs that may reactivate the remaining copy of FBXW7 in a similar way that nutlins (small-molecule MDM2-antagonists) have been shown to activate wild-type copies of p53 in human tumors (*19*). Loss of FBXW7 may also be a useful biomarker for sensitivity of human tumors to inhibitors of the mTOR pathway.

References and Notes

1. M. Welcker, B. E. Clurman, *Nat. Rev. Cancer* **8**, 83 (2008).
2. S. Akhoondi *et al.*, *Cancer Res.* **67**, 9006 (2007).
3. J. H. Mao *et al.*, *Nature* **432**, 775 (2004).
4. H. Rajagopalan *et al.*, *Nature* **428**, 77 (2004).
5. M. Yada *et al.*, *EMBO J.* **23**, 2116 (2004).
6. M. Welcker *et al.*, *Proc. Natl. Acad. Sci. U.S.A.* **101**, 9085 (2004).
7. Z. Kemp *et al.*, *Cancer Res.* **65**, 11361 (2005).
8. Single-letter abbreviations for the amino acid residues are as follows: A, Ala; C, Cys; D, Asp; E, Glu; F, Phe; G, Gly; H, His; I, Ile; K, Lys; L, Leu; M, Met; N, Asn; P, Pro; Q, Gln; R, Arg; S, Ser; T, Thr; V, Val; W, Trp; Y, Tyr; and X, any amino acid.
9. G. Wu *et al.*, *Mol. Cell. Biol.* **21**, 7403 (2001).
10. H. Strohmaier *et al.*, *Nature* **413**, 316 (2001).
11. R. M. Neve *et al.*, *Cancer Cell* **10**, 515 (2006).
12. J. Climent *et al.*, *Cancer Res.* **67**, 818 (2007).
13. K. Chin *et al.*, *Cancer Cell* **10**, 529 (2006).
14. J. Fridlyand *et al.*, *BMC Cancer* **6**, 96 (2006).
15. J. H. Mao *et al.*, *Oncogene* **22**, 8379 (2003).
16. A. Di Cristofano, B. Pesce, C. Cordon-Cardo, P. P. Pandolfi, *Nat. Genet.* **19**, 348 (1998).
17. L. S. Steelman *et al.*, *Oncogene* **27**, 4086 (2008).
18. M. Welcker, A. Orian, J. E. Grim, R. N. Eisenman, B. E. Clurman, *Curr. Biol.* **14**, 1852 (2004).
19. J. K. Buolamwini *et al.*, *Curr. Cancer Drug Targets* **5**, 57 (2005).

20. We thank B. Vogelstein for providing us with the HCT116 WT, HCT116 *FBXW7*$^{-/-}$, DLD1 wild-type, and DLD1 *FBXW7*$^{-/-}$ cell lines; K.I. Nakayama for providing *Fbxw7* knockout mice and vectors (HA-FBXW7 and HA-FBXW7ΔF); and O. Tetsu for vector encoding HA-ubiquitin. These studies were supported by NCI grant U01 CA84244 and the U.S. Department of Energy (DE-FG02-03ER63630) to A.B., the University of California at San Francisco Research-Evaluation Allocation Committee (REAC) to J.-H.M. A.B. acknowledges support from the Barbara Bass Bakar Chair of Cancer Genetics.

Supporting Online Material

www.sciencemag.org/cgi/content/full/321/5895/1499/DC1
Materials and Methods
Figs. S1 to S8
Table S1

9 July 2008; accepted 11 August 2008
10.1126/science.1162981

Unsupervised Natural Experience Rapidly Alters Invariant Object Representation in Visual Cortex

Nuo Li and James J. DiCarlo*

Object recognition is challenging because each object produces myriad retinal images. Responses of neurons from the inferior temporal cortex (IT) are selective to different objects, yet tolerant ("invariant") to changes in object position, scale, and pose. How does the brain construct this neuronal tolerance? We report a form of neuronal learning that suggests the underlying solution. Targeted alteration of the natural temporal contiguity of visual experience caused specific changes in IT position tolerance. This unsupervised temporal slowness learning (UTL) was substantial, increased with experience, and was significant in single IT neurons after just 1 hour. Together with previous theoretical work and human object perception experiments, we speculate that UTL may reflect the mechanism by which the visual stream builds and maintains tolerant object representations.

When presented with a visual image, primates can rapidly (<200 ms) recognize objects despite large variations in object position, scale, and pose (*1*, *2*). This ability likely derives from the responses of neurons at high levels of the primate ventral visual stream (*3*–*5*). But how are these powerful "invariant" neuronal object representations built

by the visual system? On the basis of theoretical (*6*–*11*) and behavioral (*12*, *13*) work, one possibility is that tolerance ("invariance") is learned from the temporal contiguity of object features during natural visual experience, potentially in an unsupervised manner. Specifically, during natural visual experience, objects tend to remain present for seconds or longer, while object motion or viewer motion (e.g., eye movements) tends to cause rapid changes in the retinal image cast by each object over shorter time intervals (hundreds of ms). The ventral visual stream could construct a tolerant object representation by taking advantage of this natural tendency for temporally contiguous retinal images to belong to the same object. If this hypothesis is correct, it might be possible to uncover a neuronal signature of the underlying learning by using targeted alteration of those spatiotemporal statistics (*12*, *13*).

To look for such a signature, we focused on position tolerance. If two objects consistently swapped identity across temporally contiguous changes in retinal position then, after sufficient experience in this "altered" visual world, the visual system might incorrectly associate the neural representations of those objects viewed at different positions into a single object representation (*12*, *13*). We focused on the top level of the primate ventral visual stream, the inferior temporal cortex (IT), where many individual neurons possess position tolerance—they respond preferentially to different objects, and that selectivity is largely maintained across changes in object retinal position, even when images are simply presented to a fixating animal (*14*, *15*).

We tested a strong, "online" form of the temporal contiguity hypothesis—two monkeys visually explored an altered visual world (Fig. 1A, "Exposure phase"), and we paused every ~15 min to test each IT neuron for any change in position tolerance produced by that altered experience (Fig. 1A, "Test phase"). We concentrated on each neuron's responses to two objects that elicited strong (object "P", preferred) and moderate (object "N", nonpreferred) responses, and we tested the position tolerance of that object selectivity by briefly presenting each object at 3° above, below, or at the center of gaze (*16*) (fig. S1). All neuronal data reported in this study were obtained in these test phases: animal tasks unrelated to the test stimuli; no attentional cueing; and completely randomized, brief presentations of test stimuli (*16*). We alternated between these two phases (test phase ~5 min; exposure phase ~15 min) until neuronal isolation was lost.

To create the altered visual world ("Exposure phase" in Fig. 1A), each monkey freely viewed the video monitor on which isolated objects appeared intermittently, and its only task was to freely look at each object. This exposure "task" is a natural, automatic primate behavior in that it requires no training. However, by means of real-time eye-tracking (*17*), the images that played out on the monkey's retina during exploration of this world were under precise experimental control (*16*). The objects were placed on the video monitor so as to (initially) cast their image at one of two possible retinal positions (+3° or −3°). One of these retinal positions was pre-chosen for targeted alteration in visual experience (the "swap" position; counterbalanced across neurons) (Fig. 1B) (*16*); the other position acted as a control (the "non-swap" position). The monkey quickly saccaded to each object (mean: 108 ms after object appearance), which rapidly brought the object image to the center of its retina (mean saccade duration 23 ms). When the object had appeared at the non-swap position, its identity remained stable as the monkey saccaded to it, typical of real-world visual experience ("Normal exposure", Fig. 1A) (*16*). However, when the object had appeared at the swap position, it was always replaced by the other object (e.g., P→N) as the monkey saccaded to it (Fig. 1A, "Swap exposure"). This experience manipulation took advantage of the fact that primates are effectively blind during the brief time it takes to complete a saccade (*18*). It consistently made the image of one object at a peripheral retinal position (swap position) temporally contiguous with the retinal image of the other object at the center of the retina (Fig. 1).

We recorded from 101 IT neurons while the monkeys were exposed to this altered visual world (isolation held for at least two test phases; $n = 50$ in monkey 1; 51 in monkey 2). For each neuron, we measured its object selectivity at each position as the difference in response to the two objects (P − N; all key effects were also found with a contrast index of selectivity) (fig. S6). We found that, at the swap position, IT neurons (on average) decreased their initial object selectivity

McGovern Institute for Brain Research and Department of Brain and Cognitive Sciences, Massachusetts Institute of Technology, Cambridge, MA 02139, USA.

*To whom correspondence should be addressed. E-mail: dicarlo@mit.edu

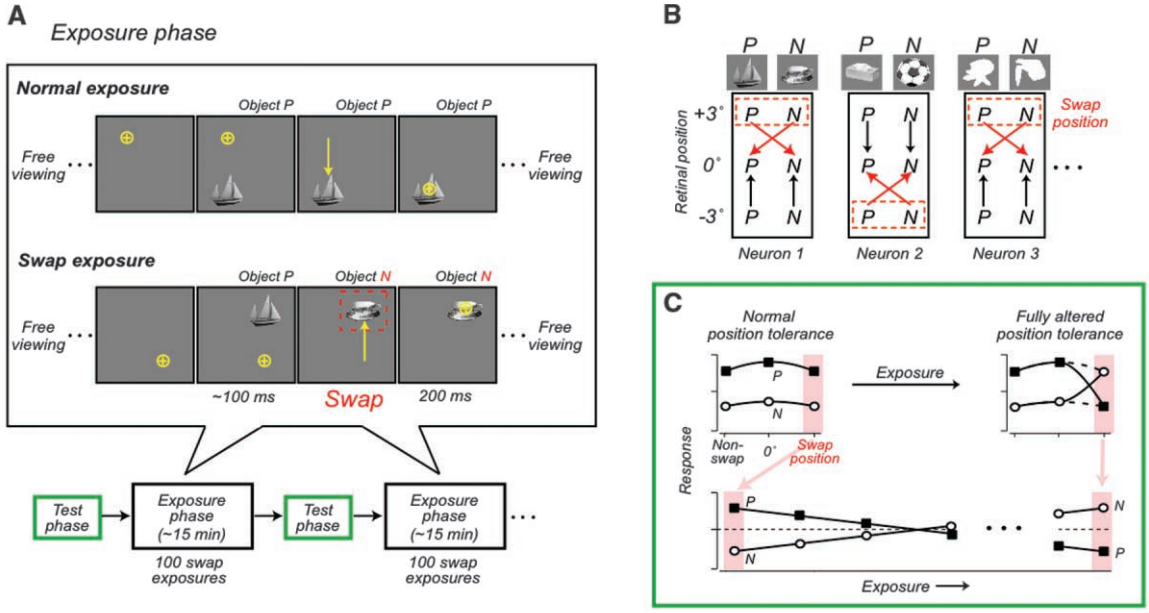

Fig. 1. Experimental design and predictions. (**A**) IT responses were tested in "Test phase" (green boxes, see text), which alternated with "Exposure phase." Each exposure phase consisted of 100 normal exposures (50 P→P, 50 N→N) and 100 swap exposures (50 P→N, 50 N→P). Stimulus size was 1.5° (*16*). (**B**) Each box shows the exposure-phase design for a single neuron. Arrows show the saccade-induced temporal contiguity of retinal images (arrowheads point to the retinal images occurring later in time, i.e., at the end of the saccade). The swap position was strictly alternated (neuron-by-neuron) so that it was counterbalanced across neurons. (**C**) Prediction for responses collected in the test phase: If the visual system builds tolerance using temporal contiguity (here driven by saccades), the swap exposure should cause incorrect grouping of two different object images (here P and N). Thus, the predicted effect is a decrease in object selectivity at the swap position that increases with increasing exposure (in the limit, reversing object preference), and little or no change in object selectivity at the non-swap position.

for P over N, and this change in object selectivity grew monotonically stronger with increasing numbers of swap exposure trials (Fig. 2, A and C). However, the same IT neurons showed (Fig. 2A) no average change in their object selectivity at the equally eccentric control position (non-swap position), and little change in their object selectivity among two other (nonexposed) control objects (see below).

Because each IT neuron was tested for different amounts of exposure time, we first computed a net object selectivity change, Δ(P − N), in the IT population by using the first and last available test phase data for each neuron. The prediction was that Δ(P − N) should be negative (i.e., in the direction of object preference reversal), and greatest at the swap position (Fig. 1C). This prediction was borne out (Fig. 3A). The position specificity of the experience-induced changes in object selectivity was confirmed by two different statistical approaches: (i) a direct comparison of Δ(P − N) between the swap and non-swap position (n = 101; P = 0.005, one-tailed paired t test); (ii) a significant interaction between position and exposure—that is, object selectivity decreased at the swap position with increasing amounts of exposure [P = 0.009 by one-tailed bootstrap; P = 0.007 by one-tailed permutation test; tests were done on (P − N)].

The changes in object selectivity at the swap position were also largely shape-specific. For 88 of the 101 neurons, we monitored the neuron's selectivity among two control objects not shown to the animals during the exposure phase (chosen similar to the way in which the P and N objects were selected, fully interleaved testing in each test phase) (*16*). Across the IT population, control object selectivity at the swap position did not significantly change (Fig. 2A), and the swap object selectivity changed significantly more than the control object selectivity (Fig. 3B) (n = 88, P = 0.009, one-tailed paired t test of swap versus control objects at the swap position).

These changes in object selectivity were substantial (average change of ~5 spikes/s per 400 exposures at the swap position) (Figs. 2C and 3C) and were readily apparent and highly significant at the population level. In the face of well-known Poisson spiking variability (*19*, *20*), these effects were only weakly visible in most single IT neurons recorded for short durations, but were much more apparent over the maximal 1-hour exposure time that we could hold neurons in isolation (Fig. 2C, lower panels). To determine if the object selectivity changes continued to grow even larger with longer periods of exposure, we next recorded multi-unit activity (MUA) in one animal (monkey 2), which allowed us to record from a number of (nonisolated) neurons around the electrode tip (which all tend to have similar selectivity) (*21*, *22*) while the monkey was exposed to the altered visual world for the entire experiment (~2 hours) (*16*). The MUA data replicated the single-unit results—a change in object selectivity only at the swap position (Fig. 2C) ("position × exposure" interaction: P = 0.03, one-tailed bootstrap; P = 0.014, one-tailed permutation test; n = 10). Furthermore, the MUA object selectivity change at the swap position continued to increase as the animal received even more exposure to the altered visual world, followed a very similar time course in the rate of object selectivity change (~5 spikes/s per 400 exposures) (Fig. 3C), and even showed a slight reversal in object selectivity (N > P in Fig. 4D).

Our main results were similar in magnitude (Fig. 3, A and B) and statistically significant in each of the two monkeys (monkey 1: P = 0.019; monkey 2: P = 0.0192; one-tailed t test). Each monkey performed a different task during the test phase (*16*), suggesting that these neuronal changes are not task dependent.

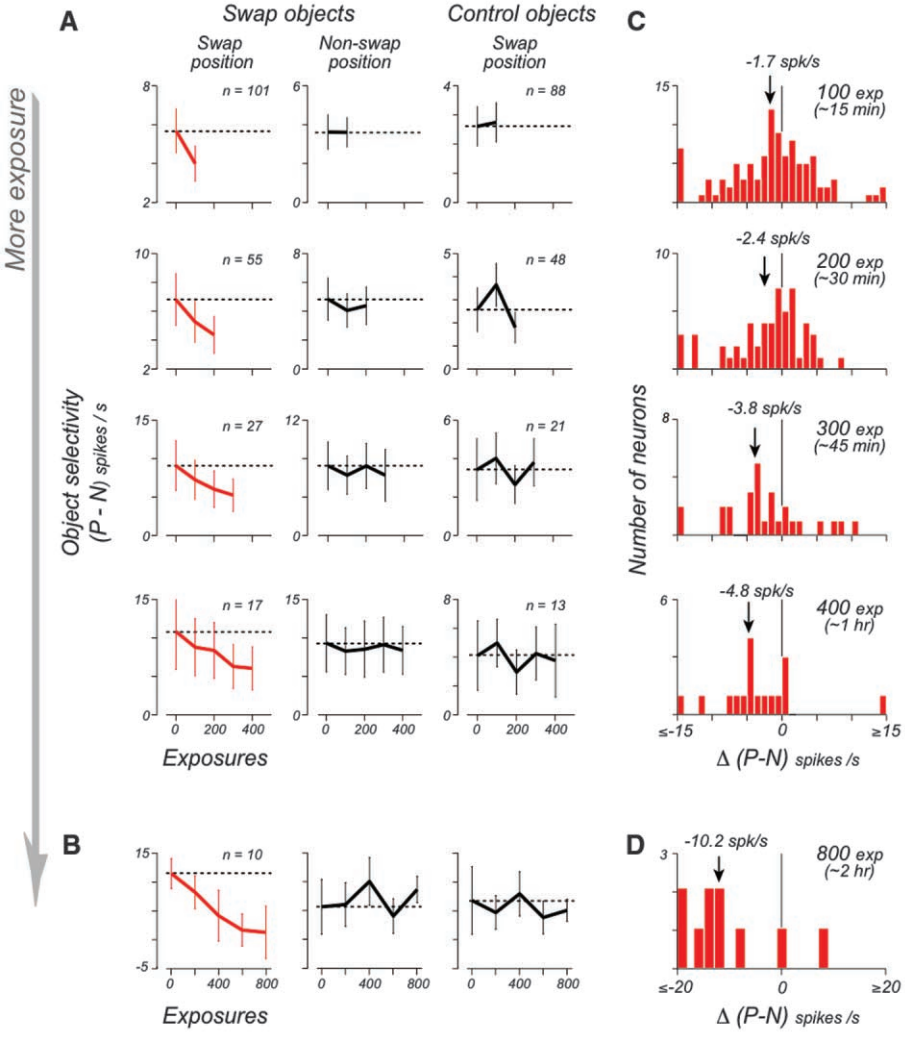

Fig. 2. Change in the population object selectivity. (**A**) Mean population object selectivity at the swap and (equally eccentric) non-swap position, and for control objects at the swap position. Each row of plots shows effect among all neurons held for at least the indicated amount of exposure (e.g., top row shows all neurons held for more than 100 swap exposures—including the neurons from the lower rows). The object selectivity for each neuron was the difference in its response to object P and N. To avoid any bias in this estimate, for each neuron we defined the labels "P" (preferred) and "N" by using a portion of the pre-exposure data (10 repetitions) to determine these labels, and the reminder to compute the displayed results in all analyses using these labels. Though there was, by chance, slightly greater initial selectivity at the swap position, this cannot explain the position specificity of the observed change in selectivity (table S2). (**B**) Mean population object selectivity of 10 multi-unit sites. Error bars (A and B) are SEMs. (**C**) Histograms of the object selectivity change at the swap position, $\Delta(P - N) = (P - N)_{\text{post-exposure}} - (P - N)_{\text{pre-exposure}}$. The arrows indicate the means of the distributions. The mean Δ(P − N) at the non-swap position was –0.01, –0.5, –0.9, and –0.9 spikes/s, respectively. The variability around that mean (i.e., distribution along the x axis) is commensurate with repeated measurements in the face of known Poisson spiking variability (fig. S11). (**D**) Object selectivity changes at the multi-unit sites. The mean Δ(P − N) at the non-swap position was 1.6 spikes/s.

Because we selected the objects P and N so that they both tended to drive the neuron (*16*), the population distribution of selectivity for P and N at each position was very broad [95% range: (−5.7 to 31.0 spikes/s) pooled across position; n = 101]. However, our main prediction assumes that the IT neurons were initially object-selective (i.e., the response to object P was greater than to object N). Consistent with this, neurons in our population with no initial object selectivity at the center of gaze showed little average change in object selectivity at the swap position with exposure (fig. S5). To test the learning effect in the most selective IT neurons, we selected the neurons with significant object selectivity [n = 52 of 101 neurons; two-way analysis of variance (2 objects × 3 positions), $P < 0.05$, significant main object effect or interaction]. Among this smaller number of object-selective neurons, the learning effect remained highly significant and still specific to the swap position ($P = 0.002$ by t test; $P = 0.009$ by bootstrap; $P = 0.004$ by permutation test).

To further characterize the response changes to individual objects, we closely examined the selective neurons held for at least 300 exposures (n = 28 of 52 neurons) and the multi-unit sites (n = 10). For each neuron and site, we used linear regression to measure any trend in response to each object as a function of exposure time (Fig. 4A). Changes in response to P and N at the swap position were apparent in a fraction of single neurons and sites (Fig. 4A), and statistically significant object selectivity change was encountered in 12 of 38 (32%) instances (Fig. 4C) (*16*). Across our neuronal population, the change in object selectivity at the swap position was due to both a decreased response to object P and an increased response to object N (approximately equal change) (Fig. 4B). These response changes were highly visible in the single-units and multi-units held for the longest exposure times (Fig. 4D).

These changes in the position profile of IT object selectivity (i.e., position tolerance) cannot be explained by changes in attention or by adaptation (fig. S10). First, a simple fatigue-adaptation model cannot explain the position specificity of the changes because, during the recording of each neuron, each object was experienced equally often at the swap and non-swap positions (also see additional control in table S2). Second, we measured these object selectivity changes with briefly presented, fully randomized stimuli while the monkeys performed tasks unrelated to the stimuli (*16*), which argues against an attentional account. Third, both of these explanations predict response decrease to all objects at the swap position, yet we found that the change in object selectivity at the swap position was due to an increase in response to object N (+2.3 spikes/s per 400 swap exposures) as well as a decrease in response to object P (−3.0 spikes/s per 400 swap exposures) (Fig. 4). Fourth, neither possibility can explain the shape specificity of the changes.

We term this effect "unsupervised temporal slowness learning" (UTL), because the selectivity changes depend on the temporal contiguity of object images on the retina and are consistent with the hypothesis that the natural stability (slowness) of object identity instructs the learning without external supervision (*6*–*11*). Our current data as well as previous human object perception experiments (*12*) cannot rule out the possibility that the brain's saccade-generation mechanisms or the associated attentional mechanisms (*23*, *24*) may also be needed. Indeed, eye-movement signals are present in the ventral stream (*25*, *26*). The relatively fast time scale and unsupervised nature of UTL may allow rapid advances in answering these questions, systematically characterizing the spatiotemporal sensory statistics that drive it, and understanding if and how it extends to other types of image tolerance (e.g., changes in object scale, pose) (*27*, *28*).

IT neurons "learn" to give similar responses to different visual shapes ("paired associates") when reward is used to explicitly teach monkeys to associate those shapes over long time scales [1 to 5 s between images; see, e.g., (*29*, *30*)], but sometimes without explicit instruction (*31*, *32*). A top-down explanation of the neuronal selectivity changes in our study is unlikely because animals performed tasks that were unrelated to the object images when the selectivity was probed, and the selectivity changes were present in the earliest part of the IT responses (~100 ms; fig S4). But UTL could be an instance of the same plasticity mechanisms that underlie "paired associate" learning; here, the "associations" are between object images at different retinal positions (which, in the real world, are typically images of the same object). However, UTL may be qualitatively different because (i) the learning is retinal position-specific; (ii) it operates over the much shorter time scales of natural visual exploration (~200 ms); and (iii) it is unsupervised in that, besides the visual world, no external "teacher" was used to direct the learning (e.g., no association-contingent reward was used, but we do not rule out the role of internal "teachers" such as efferent eye-movement signals). These distinctions are important because we naturally receive orders-of-magnitude more such experience (e.g., ~10^8 unsupervised temporal-contiguity saccadic "experiences" per year of life).

Our results show that targeted alteration of natural, unsupervised visual experience changes the position tolerance of IT neurons as predicted by the hypothesis that the brain uses a temporal contiguity learning strategy to build that tolerance in the first place. Several computational models show how such strategies can build tolerance (*6*–*11*), and such models can be implemented by means of Hebbian-like learning rules (*8*, *33*) that are consistent with spike-timing–dependent plasticity (*34*). One can imagine IT neurons using almost temporally coincident activity to learn which sets of its afferents correspond to features of the same object at different positions. The time course and task independence of UTL are consistent with synaptic plasticity (*35*, *36*), but our data do not constrain the locus of plasticity, and changes at multiple levels of the ventral visual stream are likely (*37*, *38*).

We do not yet know if UTL reflects mechanisms than are necessary for building tolerant representations. But these same experience manipulations change the position tolerance of human object perception—producing a tendency to, for example, perceive one object to be the

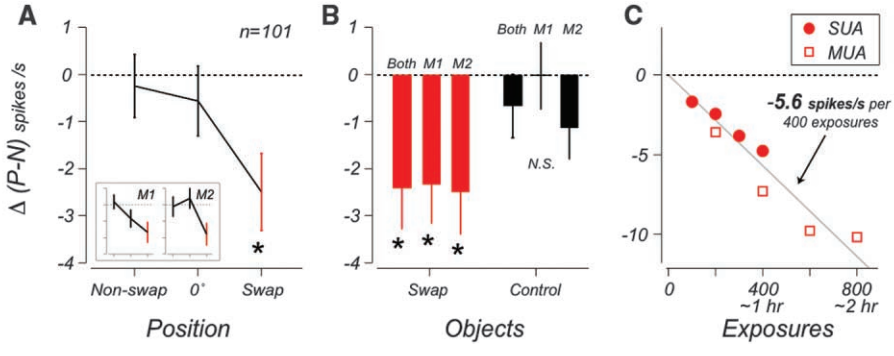

Fig. 3. Position specificity, object specificity, and time course. (**A**) Mean object selectivity change, Δ(P − N), at the swap, non-swap, and central (0°) retinal position. Δ(P − N) was computed as in Fig. 2C from each neuron's first and last available test phase (mean ~200 swap exposures). The insets show the same analysis performed separately for each monkey. (**B**) Mean object selectivity change for the (exposed) swap objects and (nonexposed) control objects at the swap position. Error bars (A and B) are SEMs. The swap object selectivity change at the swap position is statistically significant (*) in the pooled data as well as in individual animals ($P < 0.05$, one-tailed t test against 0). (**C**) Mean object selectivity change as a function of the number of swap exposures for all single-unit (n = 101) and multi-unit sites (n = 10). Each data point shows the average across all the neurons and sites held for a particular amount of time. Gray line is the best linear fit with a zero intercept; slope is mean effect size: −5.6 spikes/s per 400 exposures. The slope at the non-swap position based on the same analysis was 0.6 spikes/s (not shown).

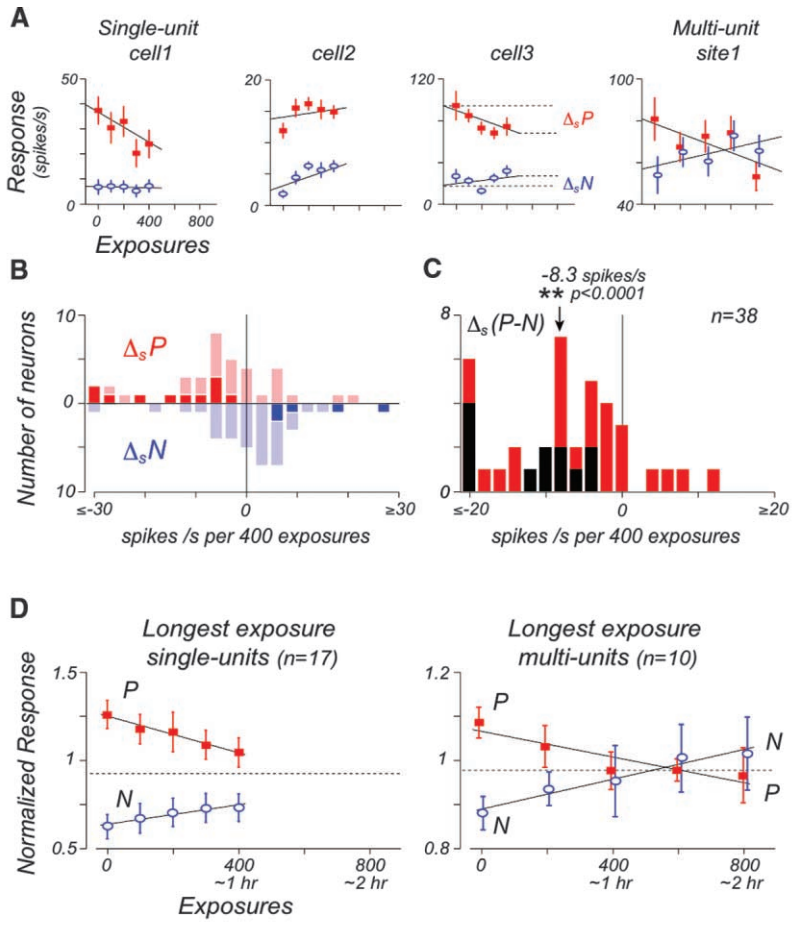

Fig. 4. Responses to objects P and N. (**A**) Response data to object P and N at the swap position for three example neurons and one multi-unit site as a function of exposure time. The solid line is standard linear regression. The slope of each line (Δ_S) provides a measure of the response change to object P and N for each neuron. Some neurons showed a response decrease to P, some showed a response enhancement to N, and others showed both (see examples). (**B**) Histograms of the slopes obtained for the object-selective neurons/sites tested for at least 300 exposures. The dark-colored bars indicate neurons with significant change by permutation test ($P < 0.05$) (*16*). (**C**) Histograms of the slopes from linear regression fits to object selectivity (P – N) as a function of exposure time; units are the same as in (B). Arrow indicates the mean of the distribution [the mean Δ_S(P – N) at the non-swap position was –1.7 spikes/s, $P = 0.38$]. The black bars indicate instances (32%; 12 of 38 neurons and sites) that showed a significant change in object selectivity by permutation test ($P < 0.05$). Results were very similar when we discarded neurons and sites with greater initial selectivity at the swap position (fig. S8). (**D**) Data from all the neurons and sites that were tested for the longest exposure time. The plot shows the mean normalized response to object P and N as a function of exposure time (compare to Fig. 1C; see fig. S3 for data at the non-swap position and for control objects). Error bars (A and D) are SEMs.

same identity as another object across a swap position (*12*). Moreover, given that the animals had a lifetime of visual experience to potentially build their IT position tolerance, the strength of UTL is substantial (~5 spikes/s change per hour)—just 1 hour of UTL is comparable to attentional effect sizes (*39*) and is more than double that observed in previous IT learning studies over much longer training intervals (*40*–*42*). We do not yet know how far we can extend this learning, but just 2 hours of (highly targeted) unsupervised experience begins to reverse the object preferences of IT neurons (Fig. 4D). This discovery reemphasizes the importance of plasticity in vision (*4*, *32*, *35*, *37*, *40*, *41*, *43*, *44*) by showing that it extends to a bedrock property of the adult ventral visual stream—position-tolerant object selectivity (*45*–*47*), and studies along the postnatal developmental time line are now needed.

References and Notes

1. S. Thorpe, D. Fize, C. Marlot, *Nature* **381**, 520 (1996).
2. M. C. Potter, *J. Exp. Psychol. (Hum. Learn.)* **2**, 509 (1976).
3. C. P. Hung, G. Kreiman, T. Poggio, J. J. DiCarlo, *Science* **310**, 863 (2005).
4. N. K. Logothetis, D. L. Sheinberg, *Annu. Rev. Neurosci.* **19**, 577 (1996).
5. R. Q. Quiroga, L. Reddy, G. Kreiman, C. Koch, I. Fried, *Nature* **435**, 1102 (2005).
6. L. Wiskott, T. J. Sejnowski, *Neural Comput.* **14**, 715 (2002).
7. P. Foldiak, *Neural Comput.* **3**, 194 (1991).
8. G. Wallis, E. T. Rolls, *Prog. Neurobiol.* **51**, 167 (1997).
9. R. Wyss, P. Konig, P. F. Verschure, *PLoS Biol.* **4**, e120 (2006).
10. T. Masquelier, S. J. Thorpe, *PLoS Comp. Biol.* **3**, e31 (2007).
11. T. Masquelier, T. Serre, S. J. Thorpe, T. Poggio, *CBCL Tech. Report #269,* Massachusetts Institute of Technology (2007).
12. D. D. Cox, P. Meier, N. Oertelt, J. J. DiCarlo, *Nat. Neurosci.* **8**, 1145 (2005).
13. G. Wallis, H. H. Bulthoff, *Proc. Natl. Acad. Sci. U.S.A.* **98**, 4800 (2001).
14. M. Ito, H. Tamura, I. Fujita, K. Tanaka, *J. Neurophysiol.* **73**, 218 (1995).
15. H. Op de Beeck, R. Vogels, *J. Comp. Neurol.* **426**, 505 (2000).
16. Materials and methods are available as supporting material on *Science* Online.
17. J. J. DiCarlo, J. H. R. Maunsell, *Nat. Neurosci.* **3**, 814 (2000).
18. J. Ross, M. C. Morrone, M. E. Goldberg, D. C. Burr, *Trends Neurosci.* **24**, 113 (2001).
19. D. J. Tolhurst, J. A. Movshon, A. F. Dean, *Vision Res.* **23**, 775 (1983).
20. M. N. Shadlen, W. T. Newsome, *J. Neurosci.* **18**, 3870 (1998).
21. K. Tanaka, *Cereb. Cortex* **13**, 90 (2003).
22. G. Kreiman *et al.*, *Neuron* **49**, 433 (2006).
23. T. Moore, M. Fallah, *Proc. Natl. Acad. Sci. U.S.A.* **98**, 1273 (2001).
24. E. Kowler, E. Anderson, B. Dosher, E. Blaser, *Vision Res.* **35**, 1897 (1995).
25. J. L. Ringo, S. Sobotka, M. D. Diltz, C. M. Bunce, *J. Neurophysiol.* **71**, 1285 (1994).
26. T. Moore, A. S. Tolias, P. H. Schiller, *Proc. Natl. Acad. Sci. U.S.A.* **95**, 8981 (1998).
27. S. Edelman, S. Duvdevani-Bar, *Neural Comput.* **9**, 701 (1997).
28. G. Wallis, H. Bulthoff, *Trends Cogn. Sci.* **3**, 22 (1999).
29. K. Sakai, Y. Miyashita, *Nature* **354**, 152 (1991).
30. A. Messinger, L. R. Squire, S. M. Zola, T. D. Albright, *Proc. Natl. Acad. Sci. U.S.A.* **98**, 12239 (2001).
31. Y. Miyashita, *Nature* **335**, 817 (1988).
32. C. A. Erickson, R. Desimone, *J. Neurosci.* **19**, 10404 (1999).
33. W. Gerstner, R. Kempter, J. L. van Hemmen, H. Wagner, *Nature* **383**, 76 (1996).
34. H. Sprekeler, C. Michaelis, L. Wiskott, *PLoS Comp. Biol.* **3**, e112 (2007).
35. C. D. Meliza, Y. Dan, *Neuron* **49**, 183 (2006).
36. H. Markram, J. Lubke, M. Frotscher, B. Sakmann, *Science* **275**, 213 (1997).
37. T. Yang, J. H. Maunsell, *J. Neurosci.* **24**, 1617 (2004).
38. Z. Kourtzi, J. J. DiCarlo, *Curr. Opin. Neurobiol.* **16**, 152 (2006).
39. J. H. R. Maunsell, E. P. Cook, *Philos. Trans. R. Soc. Lond. B Biol. Sci.* **357**, 1063 (2002).
40. C. I. Baker, M. Behrmann, C. R. Olson, *Nat. Neurosci.* **5**, 1210 (2002).
41. E. Kobatake, G. Wang, K. Tanaka, *J. Neurophysiol.* **80**, 324 (1998).
42. N. Sigala, N. K. Logothetis, *Nature* **415**, 318 (2002).
43. E. T. Rolls, G. C. Baylis, M. E. Hasselmo, V. Nalwa, *Exp. Brain Res.* **76**, 153 (1989).
44. A. Seitz, T. Watanabe, *Trends Cogn. Sci.* **9**, 329 (2005).
45. M. Dill, M. Fahle, *Percept. Psychophys.* **60**, 65 (1998).
46. M. Dill, S. Edelman, *Perception* **30**, 707 (2001).
47. T. A. Nazir, J. K. O'Regan, *Spat. Vis.* **5**, 81 (1990).

48. We thank D. Cox, R. Desimone, N. Kanwisher, J. Maunsell, and N. Rust for helpful comments

and discussion, and J. Deutsch, B. Kennedy, M. Maloof, and R. Marini for technical support. This work was supported by the NIH (grant R01-EY014970) and The McKnight Endowment Fund for Neuroscience.

Supporting Online Material
www.sciencemag.org/cgi/content/full/321/5895/1502/DC1
Materials and Methods
SOM Text
Figs. S1 to 12
Tables S1 and S2
References and Notes

5 May 2008; accepted 15 August 2008
10.1126/science.1160028

Conformational Switch of Syntaxin-1 Controls Synaptic Vesicle Fusion

Stefan H. Gerber,[1]*† Jong-Cheol Rah,[2,3]*‡ Sang-Won Min,[1]*§ Xinran Liu,[1,4] Heidi de Wit,[5] Irina Dulubova,[6] Alexander C. Meyer,[3] Josep Rizo,[6,7] Marife Arancillo,[2] Robert E. Hammer,[6,7] Matthijs Verhage,[5] Christian Rosenmund,[2,3]# Thomas C. Südhof[1,4,8]¶#

During synaptic vesicle fusion, the soluble *N*-ethylmaleimide-sensitive factor–attachment protein receptor (SNARE) protein syntaxin-1 exhibits two conformations that both bind to Munc18-1: a "closed" conformation outside the SNARE complex and an "open" conformation in the SNARE complex. Although SNARE complexes containing open syntaxin-1 and Munc18-1 are essential for exocytosis, the function of closed syntaxin-1 is unknown. We generated knockin/knockout mice that expressed only open syntaxin-1B. Syntaxin-1B^{Open} mice were viable but succumbed to generalized seizures at 2 to 3 months of age. Binding of Munc18-1 to syntaxin-1 was impaired in syntaxin-1B^{Open} synapses, and the size of the readily releasable vesicle pool was decreased; however, the rate of synaptic vesicle fusion was dramatically enhanced. Thus, the closed conformation of syntaxin-1 gates the initiation of the synaptic vesicle fusion reaction, which is then mediated by SNARE-complex/Munc18-1 assemblies.

Intracellular membrane fusion reactions are carried out by interactions between SNARE [soluble *N*-ethylmaleimide–sensitive factor (NSF)–attachment protein receptor] and SM (Sec1-Munc18–like) proteins (*1*, *2*). In Ca^{2+}-triggered exocytosis in neurons and neuroendocrine cells, fusion is catalyzed by the formation of SNARE complexes from syntaxin-1, synaptosome-associated protein of 25 kDa (SNAP-25), and synaptobrevin/vesicle-associated membrane protein and the binding of the SM protein Munc18-1 to these SNARE complexes (*1*–*3*). Syntaxin-1 consists of two similar isoforms (syntaxin-1A and -1B) that are composed of an N-terminal α-helical domain (the H_{abc} domain) and a C-terminal SNARE motif and transmembrane region. Outside of the SNARE complex, syntaxin-1 assumes a "closed" conformation, in which the H_{abc} domain folds back onto the C-terminal SNARE motif (*4*, *5*). In the SNARE complex, by contrast, syntaxin-1 is "opened" (*6*). Munc18-1 interacts with syntaxin-1 alone in the closed conformation to form heterodimers (*3*, *4*) and additionally binds to SNARE complexes containing syntaxin-1 in the open conformation to form Munc18-1– SNARE complex assemblies (*7*, *8*), which are essential for exocytosis (*3*). The function of the closed conformation of syntaxin-1 and its binding to Munc18-1 remain unknown.

We used gene targeting to create mice that lack syntaxin-1A (syntaxin-1A^{KO}) and contain the LE mutation in syntaxin-1B, which renders it predominantly open (syntaxin-1B^{Open}) (fig. S1) (*9*). Studying littermate offspring from crosses of double-heterozygous syntaxin-1A^{KO} and -1B^{Open} mice, we found that homozygous syntaxin-1A^{KO} mice exhibited no decrease in survival (Fig. 1A) or other obvious phenotypes (figs. S2 and S3). The expendability of syntaxin-1A was unexpected in view of its high concentrations and proposed central functions (*10*–*14*) and indicated that syntaxin-1A may be functionally redundant with syntaxin-1B.

Homozygous mutant syntaxin-1B^{Open} mice were also viable but severely ataxic and developed lethal epileptic seizures after 2 weeks of age (Fig. 1A and fig. S3). The seizure phenotype of syntaxin-1B^{Open} mutant mice was recessive and independent of the syntaxin-1A^{KO}. Thus, syntaxin-1B was selectively essential, probably because it is more widely expressed than syntaxin-1A (*15*). In *Caenorhabditis elegans*, transgenic syntaxin-1^{Open} rescues unc-13 mutant worms from paralysis (*16*); however, crossing syntaxin-1B^{Open} mice with Munc13-1 knockout mice did not prevent Munc13-1 knockout–induced death (fig. S4).

The syntaxin-1A^{KO} mutation abolished syntaxin-1A expression (Fig. 1B), whereas the syntaxin-1B^{Open} mutation decreased syntaxin-1B levels (Fig. 1C). Both mutations produced a modest decrease in Munc18-1 levels but no major changes in other proteins (table S1). The syntaxin-1^{Open} mutation decreases formation of the Munc18-1–syntaxin-1 complex but not formation of SNARE complexes or Munc18-1–SNARE complex assemblies (fig. S5) (*3*, *8*). Consistent with this conclusion, less Munc18-1 was coimmunoprecipitated with syntaxin-1 in syntaxin-1B^{Open} mice, whereas other SNARE proteins coimmunoprecipitated normally (Munc18-1–SNARE complex assemblies are not stable during immunoprecipitations, and thus cannot be evaluated) (Fig. 1D and fig. S6).

Electron microscopy of cultured cortical neurons from littermate syntaxin-1B^{Open} and -1B^{WT} mice lacking syntaxin-1A revealed increased vesicle docking in syntaxin-1B^{Open} synapses (~25% increase) (Fig. 2, A to D). The size of the postsynaptic density also was increased (~20%) (Fig. 2E), whereas the density of docked vesicles per active zone length was unchanged (Fig. 2F). No other structural parameter measured differed between syntaxin-1B^{Open} and -1B^{WT} synapses; in particular, the number and intraterminal distribution of vesicles were unaltered (fig. S7). In chromaffin cells, however, the syntaxin-1B^{Open} mutation caused a large decrease in chromaffin vesicle docking, similar to that of the Munc18-1 knockout. Again, neither mutation altered the total number of chromaffin vesicles (Fig. 2, K and L). Synaptobrevin-2 knockout mice, analyzed in parallel as a negative control, did not change chromaffin vesicle docking but did increase the total number of chromaffin vesicles (Fig. 2L). Consistent with earlier findings (*17*–*20*), these results indicate that the Munc18-1–syntaxin-1 complex, but not the SNARE complex, functions in chromaffin vesicle docking. This function may not be apparent in vertebrate synapses because active zone proteins that are absent from chromaffin cells probably dock synaptic vesicles independent of their attachment to the Munc18-1–syntaxin-1 complex.

Measurements of spontaneous miniature excitatory postsynaptic currents (mEPSCs), excitatory postsynaptic currents (EPSCs) evoked by

[1]Department of Neuroscience, University of Texas Southwestern Medical Center, Dallas, TX 75390–9111, USA. [2]Department of Molecular and Human Genetics and Department of Neuroscience, Baylor College of Medicine, Houston, TX 77030, USA. [3]Department of Membrane Biophysics, Max-Planck-Institute for Biophysical Chemistry, 37077 Göttingen, Germany. [4]Department of Molecular Genetics, University of Texas Southwestern Medical Center, Dallas, TX 75390–9111, USA. [5]Department of Functional Genomics, Vrije Universiteit, 1081 Amsterdam, Netherlands. [6]Department of Biochemistry, University of Texas Southwestern Medical Center, Dallas, TX 75390–9111, USA. [7]Department of Pharmacology, University of Texas Southwestern Medical Center, Dallas, TX 75390–9111, USA. [8]Howard Hughes Medical Institute, University of Texas Southwestern Medical Center, Dallas, TX 75390–9111, USA.

*These authors contributed equally to this work.
†Present address: Abteilung Innere Medizin III, Universität Heidelberg, 69120 Heidelberg, Germany.
‡Present address: Developmental Synaptic Plasticity Section, National Institute of Neurological Disorders and Stroke, Bethesda, MD 20892, USA.
§Present address: University of California, San Francisco, Mission Bay Campus, San Francisco, CA 94158, USA.
¶Present address: Department of Molecular and Cellular Physiology and Neuroscience Institute, Stanford University, Palo Alto, CA 94304–5543, USA.
#To whom correspondence should be addressed. E-mail: rosenmun@bcm.tmc.edu (C.R.); tcs1@stanford.edu (T.C.S.)

Supporting Online Material

Materials and methods

Supporting text

Supporting figures

Supporting tables

Materials and methods

Animals and surgery

Experiments were performed on two male rhesus monkeys (Macaca mulatta, 5.6 and 4.3 kg). Aseptic surgery was performed to implant a head post and a scleral search coil. After brief behavioral training (1-3 months), a second surgery was performed to place a recording chamber (18 mm diameter) to reach the anterior half of the temporal lobe. All animal procedures were performed in accordance with National Institute of Health guidelines and the Massachusetts Institute of Technology Committee on Animal Care.

Stimuli presentation and behavioral task

Each recorded neuron was probed in a dimly lit room with a set of 100 achromatic images of isolated objects (52 natural objects and 48 silhouette white shapes; Fig. S2) presented on a gray background (21" CRT monitor, 85 Hz refresh rate, ~48cm away, background gray luminance: 22 Cd/m^2, max white: 46 Cd/m^2). All objects subtended ~1.5º (average of a bounding square and the filled area). Custom software controlled the stimulus presentation and behavioral monitoring. Eye position was monitored in nearly real-time using standard sclera coil technique (*2*), and saccades >0.2° were reliably detected (*1*) .

During each *Test Phase* (~4 minutes), neuronal selectivity at three retinal positions (-3º, 0º, +3º elevation; all 0º azimuth) was probed in two different tasks. Monkey 1 freely searched an array of eight small dots (size 0.2º) vertically arranged 3º apart (Fig. S1). The dots never changed in appearance, but on each "trial", one dot was randomly baited in that a juice reward was given when the animal foveated that dot, and the next "trial" continued uninterrupted. Typically, the monkey saccaded from one dot to another (not always the closest dot) looking for the hidden reward. During this task, objects were presented (100 ms duration) at controlled retinal positions (onset time was the detected end of a saccade; approximately one such presentation every other saccade, never back-to-back saccades). The monkey's task was unrelated to these test stimuli. To limit unwanted experience across retinal positions, each such presented object was immediately removed upon detection of any saccade, and these aborted presentations were not included in the analyses. Monkey 2 performed a more standard fixation task in which it foveated a single, central dot (size 0.2º, ±1.5º fixation window) while object images were presented at a natural, rapid rate (5 images/s; 100 ms duration, 100 ms blank intervals). Reward was given at trial end (5-8 images presented per trial). Upon any break in fixation, any currently present object image was immediately removed (and not included in the analyses), and the trial aborted. The animal successfully maintained fixation in 75% of the trials. The presentations before the broken fixation were included in the analyses. To address possible adaptation concerns, we re-performed the key analysis after discarding the first image presentation in each fixation trial, and the result was essentially unchanged (also see Fig, S8). Aside from the task differences (free-viewing search vs. fixation), retinal stimulation in the two tasks was essentially identical in that each tested object image was presented 3º above, below or on the current center of gaze, for 100 ms duration (20-30 pseudo-randomly interleaved repetitions of each). Given equivalent retinal

stimulation, IT neuronal responsivity and selectivity are virtually identical when measured during free viewing and fixation (*1*). Consistent with this, we found comparable exposure-induced changes in IT object selectivity in each animal (e.g. see Fig. 3).

During each *Exposure Phase* (~15 minutes), animals freely viewed the monitor while object images were intermittently (~13 per minute) presented (pseudo-randomly) at +3º and -3º (always relative to the current center of gaze). The onset of each object was ~65 ms (randomly chosen between 30-100 ms) after the end of a saccade (defined by eye velocity < 10º/s). Because foveating a suddenly appearing object is a natural, automatic behavior, essentially no training was required, and the monkeys almost always saccaded directly to the object (>90%) within 108 ms (median; range: 66-205 ms) and foveated it for >200 ms (after which it was removed and the monkeys received a drop of juice). For objects presented at the "swap" position (+3º or -3º; strictly alternated neuron-by-neuron), the object (e.g. "P") was consistently swapped by another object (e.g. "N") upon the detection of saccade onset (eye speed > 60º/s). We took great care to ensure the spatiotemporal precision of the stimuli delivery. The to-be-swapped object was always successfully removed before the end of the saccade, and the new object was present at the to-be-center of the retina within 1 ms of the saccade end (mean; worst case was 10 ms after saccade end). To prevent unintended retinal experience, the object image was automatically taken away if the saccade was not directed toward the object, or if the eye landed more than 1.5º away from its center.

Neuronal recordings

The extra-cellular spiking activity of single, well-isolated IT neurons was recorded using standard microelectrode methods (*1*). 101 neurons were randomly sampled over a ~4x6 mm area of the ventral STS and ventral surface lateral to the AMTS (Horsey-Clark coordinates: AP 11-15 mm; ML 15-21 mm at recording depth) from the right hemisphere of Monkey 1 and left hemisphere of Monkey 2. In each daily recording session, we advanced a microelectrode while the 100 object images (Fig. S2) were pseudo-randomly presented at the center of gaze while the monkey performed either the free-viewing search task or the fixation task (see *Test Phase* above). All responsive neurons with a well-isolated waveform were further probed with the same object set (initial screening of 100 objects, ~5 repetitions per object, all presented at the center of gaze).

Main test objects ("swap" objects): Among the objects that drove the neuron "significantly" above its background response (t-test against 50 ms epoch before stimuli onset, $p < 0.05$, not corrected for multiple tests), the most preferred (P) and least preferred (N) objects were chosen as a pair for the *Exposure Phase* ("swap objects") subject to the condition that both objects were either from the "natural" object set or the "silhouette" object set (see Fig. S2). This object selection procedure aims to find conditions in which *both* objects drive the neuron, and object P drives the neuron more strongly than object N. For most neurons, object N was not the second most preferred object (IT neurons typically respond well to ~10% of object images, which is consistent with our online observation that N was roughly the tenth most preferred object in the set of 100 tested objects). Note that, because the procedure for choosing objects P and N was

based on limited initial testing, it does not fully guarantee that the selectivity will be found with further testing (see main text). Furthermore, because the initial testing was at the center-of-gaze position and IT neurons are not uniformly position tolerant, the procedure also does not guarantee that the response to P is greater than N at all three tested positions (i.e. possible "negative" object selectivity at some positions). We use post-hoc analysis and screening to examine any unexpected effects of this screening procedure (e.g. post-hoc removal of neurons with low or negative selectivity, table S1). Post-hoc analyses also showed that roughly equal numbers of neurons were recorded using swap objects from each set (57 natural, 44 silhouette) and neurons showed virtually the same reported changes in object selectivity when sorted by object set type.)

Control objects: For each recorded neuron, we also used the initial response testing (above) to choose a pair of control objects. Our goal was to choose these two objects among which the neuron was selective, but were very distant from the "swap objects" in shape space. Because we do not know the dimensions of shape space, we cannot strictly enforce this. In practice, we simply insured that the control objects were always chosen from the object set that was not used for the swap objects (i.e. when two objects from the "natural" set were used as "swap" objects, the two control objects were from the silhouette set, see Fig. S2). Within this constraint, the control objects were chosen using the exact same responsivity and selectivity criteria as the test objects (above).

Once the initial screening and object selection were completed, we carried out the *Test* and *Exposure Phase* in alternation for as long as we could maintain isolate of the neuron's waveform. Both swap objects and control objects were presented (tested) at all three positions during each *Test Phase* but only the swap objects were shown and manipulated during each *Exposure Phase*.

In addition, multiple-unit activity (MUA) was collected from 10 sites on the IT ventral surface of Monkey 2 on 10 different experimental sessions (days). Nearby IT neuron have similar object selectivity (*3*) and, consistent with this, we have previously shown that MUA is shape selective and moderately position tolerant (*4*). MUA was defined as all the signal waveforms in the spike band (300 Hz – 7 kHz) that crossed a threshold set to ~2 s.d. of the background activity. The threshold was held constant for the entire session. All other recording procedures were identical to the recording procedure used for the single-unit recording except: 1) during the *Test Phase*, more repetitions (~50) were collected per object image at each position; 2) each *Exposure Phase* was approximately twice as long (e.g. 200 "swap" exposures instead of 100).

Data analysis

To get the most statistical power from the data, average firing rates were computed over a time window optimally chosen for each neuron by an algorithm that estimated neuronal response onset and offset time (relative to stimulus onset) using all stimuli (see below). Analyses for the single-unit data in the main text were performed using such neuron-specific spike count windows (described next). All analyses were also repeated using a standard, fixed spike count window (onset 100 ms; offset 200 ms) with very similar results (Δ_S(P-N) = -5.4 spikes/s per 400

exposures at the swap position; -0.3 at the non-swap position; $p < 0.01$, "position x exposure" interaction by permutation test).

Neuronal response window: Specifically, for the single-unit data, each neuron's responses to each stimulus condition were computed over the same spike count time window. That window was optimally chosen for each neuron using the following algorithm (*5*). Given a neuron, we first computed its average firing rate profiles $FR_{obj}(t)$ in overlapping time bins of 25 ms shifted in time steps of 1 ms. This averaged firing rate was computed with all the response data to all the objects presented in all *Test Phases* for the neuron. We also computed the neuron's background rate FR_{bk} as the mean spike rate between 0 and 50 ms after stimulus onset. Because multiple images were presented on each trial at a relatively rapid rate (see above), the more standard epoch before each stimulus onset was not ideal for computing background because it was occupied by the neuron's response to the previous stimulus. We previously found that the short epoch starting at stimulus onset and ending before the neuronal response (i.e. before the known IT latency) provides the most reliable estimate of a "background" firing rate (*5*). Then, by subtracting this background rate from the averaged object response rate profile, we obtained an averaged driven rate profile $FR_{driven}(t) = FR_{obj}(t) - FR_{bk}$. Finally, we identified the samples for which $FR_{driven}(t)$ was at least 20% of its peak value. The largest continuous interval of samples fulfilling this requirement was always centered on the peak of the neuronal response. If no other samples, outside this main "peak" interval, fulfilled the requirement, the extremes of the interval were chosen as the extremes of the optimal spike count window for that neuron. If the firing profile exceeded 20% of its peak in other regions of the time axis, these were merged with the main interval only if they were within 25 ms from it. In this case, the extremes of the merged interval were chosen as the extremes of the optimal spike count window. In principle this algorithm could yield a very small response window, so we limited that possibility by imposing a minimum response window size of 50 ms at the estimated onset latency. (In practice, only two neurons out of 101 had this minimum window size imposed; neuron1: 30ms; neuron2: 40ms). All analyses presented in the main text were carried out by counting spikes in these neuron-specific optimized time windows. The mean window start time (± s.d.) was 119.5 ± 38 ms, the mean window end time was 244 ± 76 ms, and the median duration was 110 ± 50 ms. These time windows are consistent with previous work (*6*) and with animal reaction times in recognition tasks (*7*).

For the multi-unit data, we used a standard, fixed (100-200 ms) spike count time window for all recording sites.

For all the results presented in the main text, the object selectivity for an IT neuron was computed as the difference in its response to object P and N. To avoid any bias in this estimate of selectivity, for each neuron we defined the labels "P" and "N" by splitting the pre-exposure response data and used a portion of it (10 response repetitions to each object at each position) to determine these labels ("P" is the preferred object that elicited a bigger overall response pooled across position). The label "P" and "N" for the neuron was then held fixed across positions and later *Test Phases*. All remaining data were used to compute the selectivity results in the main text using these labels. This procedure ensured that any observed response difference between object P and N reflected true selectivity for a neuron, not selection bias.

In cases when neuronal response data is normalized and combined (e.g. Figs. 4D, S3, S9), we used the same normalization scheme through out all the analyses. Specifically, each neuron's response from each *Test Phase* was normalized to its mean response to all objects at all positions in that *Test Phase*.

Statistical tests for the "Position x Exposure" interaction

A key part of the prediction is that any change in object selectivity should be found predominantly at the swap position (Fig. 1C). Individual t-tests show a highly significant effect at the swap position, but no significant effect at the non-swap position (see Fig. 3A). However, to directly test for an interaction between position and our independent variable (exposure), we applied a general linear model to the response difference (in firing rate) between the object P and N. The formulation is similar to the analysis of variance tests (ANOVA). However, it is not subject to assumptions about the noise distributions.

The model had the following form:

$$(P-N)_{\substack{neuron=n \\ position=p \\ exposure=e}} = a_n + (b_1 \cdot p) + (b_2 \cdot e) + (b_3 \cdot (p \cdot e))$$

The three independent variables of the model are: position (p), exposure (e), and their interaction (i.e. their product, $p \cdot e$). The position factor has two levels (i.e. p = -1 for swap position, 1 for non-swap position) the exposure factor has up to 5 levels depending how long a neuron was held, (i.e. e = 0 for pre-exposure, and can be up to 400 exposures in increments of 100's,). Each a_n is the selectivity offset specific to each neuron; b_1, b_2, and b_3 are slope parameters that are shared among all the neurons. Thus, the complete model for our population of 101 neurons contained a total of 104 parameters (101 a_n's, b_1, b_2, and b_3) that were fitted simultaneously to our entire data set. The a_n's absorb neuron-by-neuron selectivity differences that are not of interest here, and the remaining three parameters describe the main effects in the population, with b_3 of primary interest (interaction).

To test for a statistically significant interaction, we fit the linear model to the data (standard least squares), and then asked if the observed value of the interaction parameter (b_3) was statistically different from 0. The validity of the significance was verified by two different approaches: 1) bootstrap and 2) permutation test.

Bootstrap is widely used to provide confidence intervals on parameter estimates. However, the bootstrap confidence interval can also be used to provide a significance level for a hypothesis test (*8*). To do this, we estimated the distribution of the b_3 estimate via a bootstrap over both neurons and repetitions of each neuron's response data. The exact procedure was done as follows: for each round of bootstrap over neurons, we randomly selected (with replacement) 101 neurons from our recorded 101 neurons, so a neuron could potentially enter the analysis multiple times. Once a set of neuron was selected, we then randomly selected (with replacement) the response repetitions included of each neuron (our unit of data is a scalar spike rate in response to

a single repetition of one object at one position). Each neuron's (P-N) was computed from its selected response repetitions. The linear model was then fit to the data at the end of these two random samples to obtain a new b_3 value. This procedure was repeated 1000 times yielding a distribution of b_3 values, and the final p-value was computed as the fraction of times that distribution is less than 0 ($p = 0.009$, 1000 samples). This p-value is interpreted as: if we were to repeat this experiment, with both the variability observed in the neuronal responses as well as the variability in which neurons were sampled, what is the chance that we would *not* see the interaction observed here? In effect, the bootstrap analysis determined the confidence interval around our originally observed b_3 value, and the duality of confidence intervals and hypotheses testing allowed us to report that confidence interval as a p value (*8*). When the same analysis was applied to the pair of control objects that was included in the *Test Phase* but was not shown during the *Exposure Phase*, we did not observe a significant interaction ($p > 0.05$). Simulations with Poisson spiking neurons have confirmed the correctness of our analysis code.

To further confirm statistical significance level of the interaction (position x exposure) by permutation test, we created a null distribution by randomly permuting the position labels of the original data points (swap vs. non-swap) from each exposure level. Following each permutation, we fit the linear model to the permuted response data. Repeating this, we determined the fraction of times that the interaction term (b_3) was greater the observed value and took this as the p value ($p = 0.007$, one-tailed test, 1000 samples). Again, when we applied the same test to the response data to the control objects, we did not observe a significant interaction ($p > 0.05$).

Together, our statistical tests point to a position-specific change in object selectivity at the swap position that increases with amount of exposure. The same statistical tests were applied to the multi-unit data ($n = 10$ sites), also yielding a significant interaction between position and exposure ($p = 0.03$ bootstrap, $p = 0.014$ permutation test) for the swap objects. Again no such interaction was observed for the control objects ($p > 0.05$ for both bootstrap and permutation test).

Statistical tests for the response change in single neurons/sites

In Fig. 4B and C, we evaluated each single-unit-neuron/multi-unit-site's response change to P, N or (P-N) by fitting linear regression as a function of exposure time to obtain a slope (Δ_SP, Δ_SN, or Δ_S(P-N)). The statistical significance of the response change for each single-unit neuron or multi-unit site was evaluated by permutation test. Specifically, for each neuron, we randomly permutated the exposure level label for each response sample, (i.e. which *Test Phase* each sample of P and N belongs to). We then re-fit the linear regression to the permuted data and repeated the same procedure 1000 times yielding a distribution of slopes ("null distribution"). The p value was determined by counting the faction of time the null distribution exceeded the linear regression slope obtained from the data. All neuron/sites with $p < 0.05$ was deemed significant (dark colored bars in Fig. 4B and C).

Supporting text

Relationship between learning effect size and IT neurons' object selectivity at the center of gaze

Implicit in our experimental design and hypothesis is that the IT neurons prefer object P over N. Indeed, object selectivity at the center of gaze may provide the "driving force" for the temporal-continuity learning in our experiment. Thus, if all our IT neurons had no selectivity among the objects P and N, then the temporal-continuity learning hypothesis makes no clear prediction in our data. On average, our recorded IT neurons did have the desired net positive object selectivity (Table S1). However, even though we aimed to pick objects so that P > N, we used an initial screen that mainly sought to insure that *both* objects P and N tended to drive the neuron (see main text and Materials and methods, above). As a result, the population distribution of selectivity for P and N at each position was very broad, and some neurons did not have clear object selectivity at the center of gaze. Here we consider subsets of IT neurons with ever-more stringent positive object selectivity at the center of gaze by re-performing our key statistical analyses on these subsets. In sum, the main results are unchanged: 1) as with the entire population, these subsets of selective neurons show a significant interaction between position and exposure time, (see details of this statistical test in Materials and methods, above); 2) as with the entire population, these subsets of selective neurons show a significant shift in their mean object selectivity (P-N) at the swap position compared to the non-swap position (pair-wise t-test). These results are summarized in Table S1.

To examine whether a relationship exist between the IT neuron's selectivity at the center of gaze and the magnitude of the learning effect, we divided the neurons (n = 101) into sub-populations based on each neuron's selectivity for P and N at the center of gaze (Fig S5). Examining the magnitude of the learning effect across these sub-populations of neurons revealed two things: 1) neurons with no or negative selectivity, on average, produced no learning effect (effect size = -0.8 spikes/s per 400 exposures); 2) effect size grew increasingly stronger among neurons with higher initial object selectivity at the center of gaze. This is consistent with the notion that selectivity at the center of gaze may be a good estimate of the "driving force" for the learning effect. Expected Poisson spiking variability in the neuronal responses prevented us from determining if this measure is a perfect predictor of the learning effect size, but we speculate that the learning effect size in each neuron cannot be simply predicted from object selectivity at the center of gaze alone, but probably also depends on (e.g.) its initial response magnitudes at the swap position.

The object selectivity change is robust to the choice of selectivity metric

Is the change in object selectivity reported here robust to the choice of metric quantifying it? In the main text, we performed all the analyses by quantifying the object selectivity in raw response difference (spikes/s). Here we explore another standard selectivity metric and show the reported results is un-affected by the choice of metric.

Specifically, for each neuron we computed a "contrast" object preference index (OPI) at each position using a standard metric (*9, 10*) :

$$OPI = \frac{P - N}{P + N}$$

where P and N is the neuron's response to object P and N. OPI ranges from -1 to +1 and 0 is no object selectivity. We computed each neuron's change in object selectivity magnitude as:

$$\Delta OPI = OPI_{post-\exp osure} - OPI_{pre-\exp osure}$$

The re-make of main text Fig. 3 using the OPI metric is shown in Fig. S6. To weight all neurons approximately equally before pooling, the ΔOPI in Fig. S6 was normalized for each neuron to its pre-exposure object selectivity:

$$\text{Normalized } \Delta OPI = \frac{\Delta OPI}{(OPI_{pre-\exp osure} + 1)}$$

Because the OPI metric ([-1 1]) can have occasionally near-zero or negative values, the addition of one in the denominator was used to regularize the normalization.

Dependence of effect size on initial object selectivity

We considered the possibility that the observed change in object selectivity at the swap position (but not at the non-swap position) might somehow have resulted from larger (or smaller) initial object selectivity magnitude at that position (relative to the non-swap position). Because we changed the swap and non-swap position across each recorded neuron, position is counter-balanced across neurons so, in the limit, no difference in initial object selectivity magnitude is expected. Indeed, the initial object selectivity was very closely matched between the swap and non-swap positions across the neuronal population (Fig S7).

However, even with the counterbalance, it turned out that our recorded population had a slightly greater initial selectivity at the swap position (by ~ 2 spikes/s in (P-N); Table S2). This difference between the swap and non-swap position was not significant ($p > 0.05$, two-tailed t-test). Nevertheless, to fully control for any effect of this slight difference on our results, we performed a post-hoc analysis to completely match the initial object selectivity. Specifically, we discarded neurons with significantly greater selectivity (P-N) at the swap position ($p < 0.05$, one-tailed permutation test), and then re-performed the key analyses on the remaining population. This re-analysis was done for the population of all 101 neurons in Fig. 2 & 3 and for the population of 38 highly-object-selective neurons/sites in Fig 4C. The results showed that our post-hoc selection had completely eliminated the small bias in initial selectivity at the two positions, but the effect size at the swap position in the "equalized" populations was almost as the original populations (and still no effect at the non-swap position; see Table S2 and Fig. S8).

Finally, by sorting the neurons based on their response profile across positions, we found that even neurons that initially were less responsive at the swap position showed a change in object selectivity (Fig S9 – especially see panel B).

The object selectivity change cannot be explained by "adaptation"

When repeatedly probed with visual stimuli, neurons in ventral visual stream have been shown to reduce their evoked responses, a phenomenon referred to as "adaptation" (*11-15*). Our IT neuronal data do show evidence of "adaptation" (outlined below). However, the key changes in IT selectivity we report in this manuscript cannot be explained by "adaptation". First, although each object was shown equally often at the two key positions (swap and non-swap positions), the selectivity change we found was specific to the swap position. This specificity cannot be explained by any standard model of "adaptation". Second, approximately half of the selectivity change was due to an enhanced response to object N (see main text), which is inconsistent with any fatigue-adaptation model. Third, the selectivity change we found continued to grow larger and larger for as long as we could measure it (up to two hours),which is suggestive of plasticity, rather than cortical fatigue.

Consistent with previous reports on IT "adaptation" (*11-15*), we observed a reduction in the neurons' responses over short time scales (i.e. within a trial, ~1 sec) and intermediate time scales (i.e. within a *Test Phase*, ~4 min). Such reduction was not specific to objects or position (Fig S10A and B). However, the change in selectivity we report here emerged slowly over a much longer times scale (across multiple *Test Phases*), and was specific to both the swap position and the object (Fig S10 C). Interestingly, there was virtually no change in response across the longer time scale over which the learning effect emerged (e.g. non-swap position, Fig. S10 right panel of row C).

Monte Carlo simulations with Poisson spiking neurons

Beyond the main (net) change in object selectivity reported here, our figures show that many individual neurons *appear* to undergo changes in object selectivity in both the predicted and non-predicted directions (e.g. scatter of the individual neurons in Fig 2C). Is this non-predicted variability in the observed object selectivity accounted for by Poisson variability (i.e. noise effects on repeat measurements)?

To address this question, we ran Monte Carlo simulations using Poisson spiking statistics. We first computed each neuron's mean firing rates to each object at each position before any exposure. Using these estimated firing rates, we simulated Poisson spiking neurons. We then took repeated measurements from this simulated population of neurons. 30-50 response repetitions were collected from each simulated neuron to constitute a simulated *Test Phase*, (matched to the number of response repetitions collected from real neurons/sites). Each

simulated neuron was then tested across the same amount of exposure time (i.e. number of *Test Phase*) as the real neurons.

In the simulations, we assumed that the object selectivity for P and N at the swap position was changing at the rate estimated from the data (5.6 spikes/s per 400 exposures, see Fig. 3C) and not changing at the non-swap position. That is, the simulated neurons' firing rates at the non-swap position were held fixed at each simulated Test Phase, while the firing rates at the swap position were undergoing changes at -0.7 spikes/s for object P and +0.7 spikes/s for object N across each *Test Phase* (100 exposures).

This simulation allowed us to determine the expected variability in a real neuronal population's selectivity under Poisson firing statistics. Finally, we compared this expected variability to that observed in our data by plotting the results together (Fig. S11). These Monte Carlo simulations showed that the magnitude of the non-predicted changes in object selectivity is comparable to that expected from well-established cortical neuron Poisson spiking statistics (*16, 17*).

Supporting figure S1

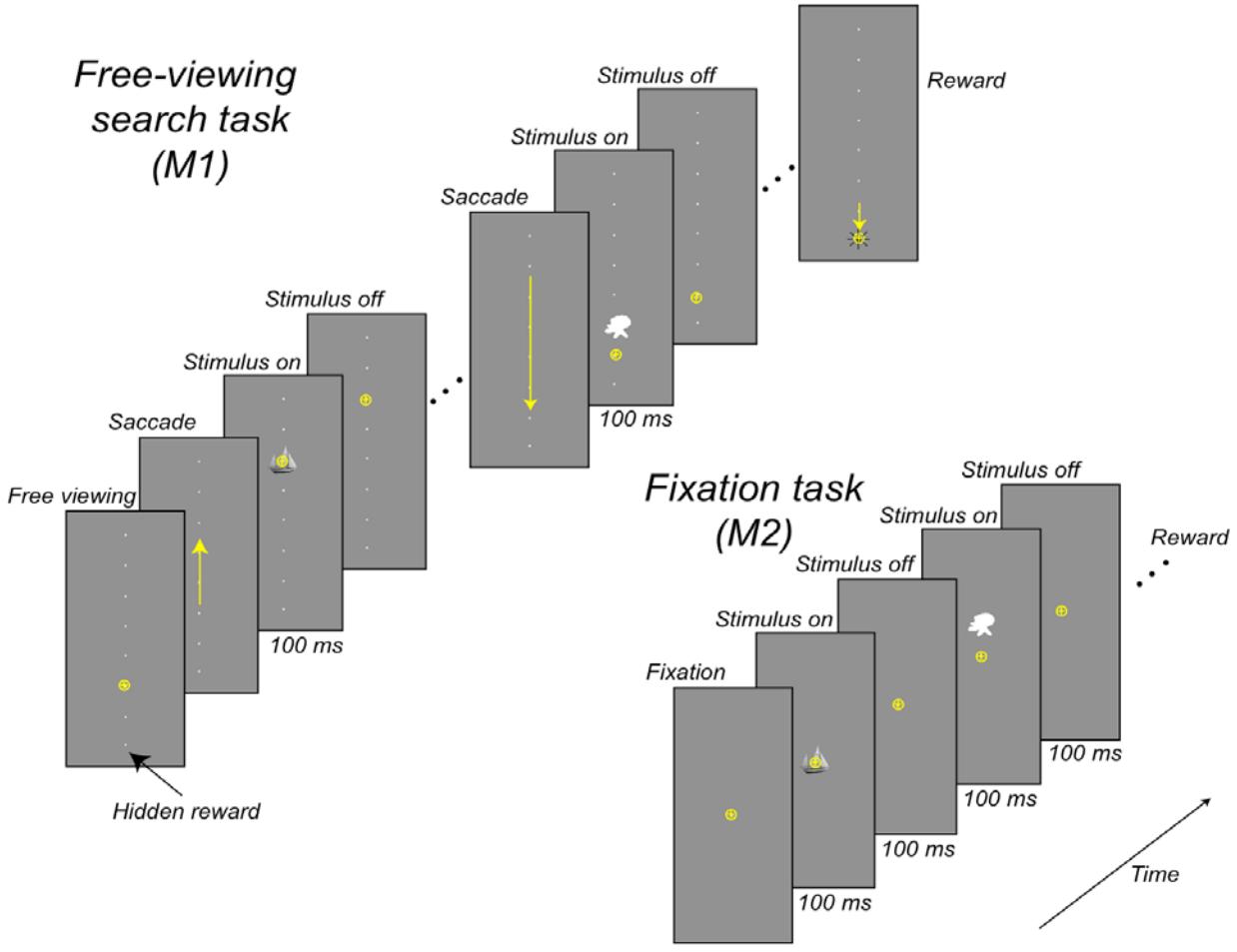

Fig. S1. Monkey tasks during neuronal testing. During the *Test Phase* of the experiment, Monkey 1 performed a free-viewing search task, searching for a reward "hidden" beneath one of eight, spatially fixed dots; Monkey 2 performed a standard, fixation task while stimuli were presented at a rate of 5 per second (100 ms duration, 100 ms gaps). In both cases, retinal stimulation for the presentation of each object image was identical in that object images were presented 3° above, 3° below, or at the center of gaze for 100 ms. In both cases, these object image presentations were fully randomized and unrelated to the animals' tasks. Each animal also performed its *Test Phase* task while we advanced a microelectrode to search for neurons, but object images were only presented at the center of gaze in that case.

Supporting figure S2

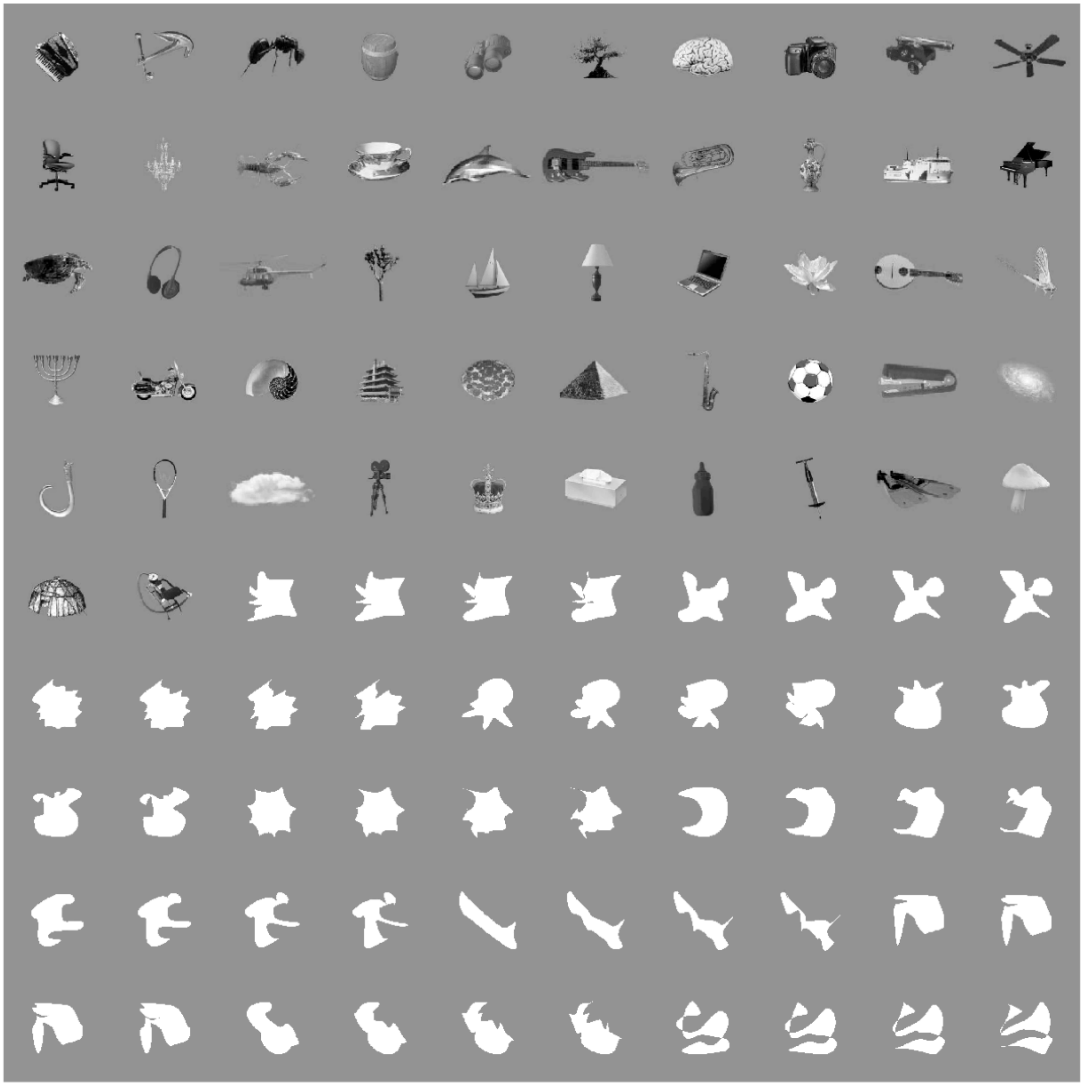

Fig. S2. Set of 100 object stimuli. The figure reflects the true relative size of the objects shown in the experiment. The first 52 images are referred to as the "natural" object set, the latter 48 images as the "silhouette" object set. We only swapped pairs of objects draw from within the same set (see Materials and methods).

Supporting figure S3

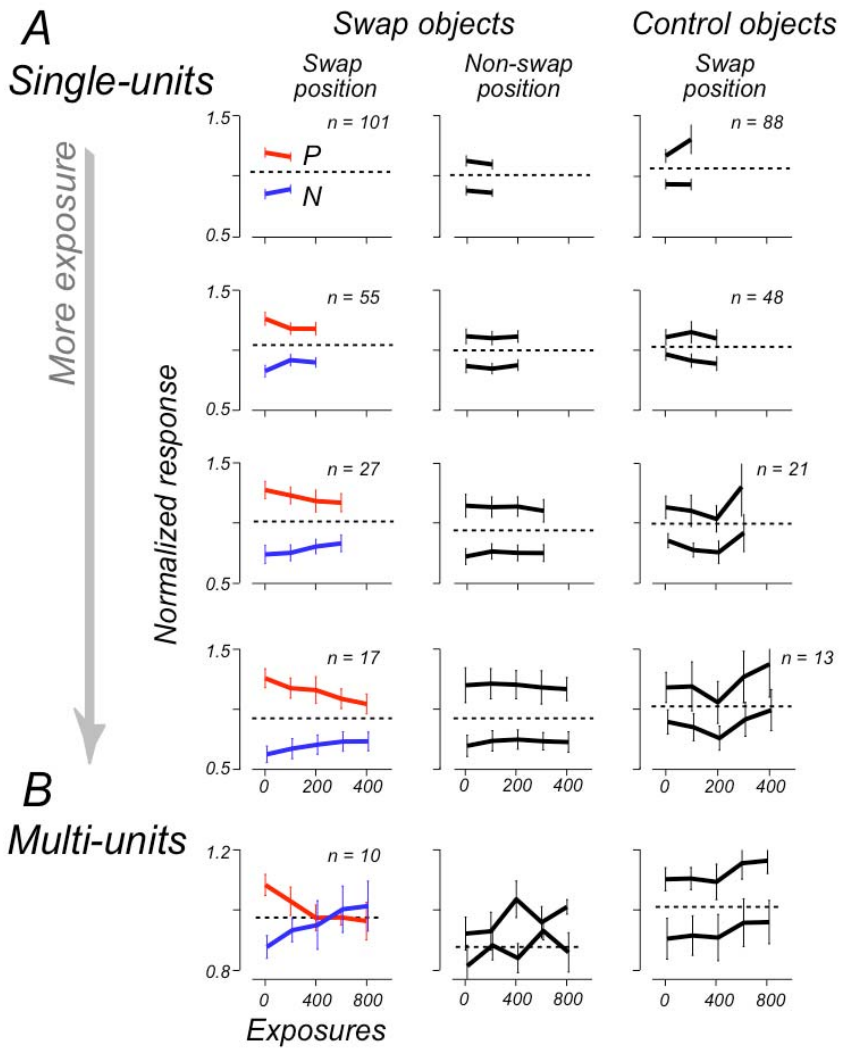

Fig. S3. Mean normalized population response to object P and N as a function of exposure time. (**A**) Single-unit population data. Each row of plots show neurons held for different amounts of time, (e.g. the top row shows all neurons held for over 100 swap exposures -- including the neurons from the lower rows; the second row shows the neurons held for over 200 exposures; etc). Each neuron's response from each *Test Phase* was normalized to its mean response to all objects at all positions in that *Test Phase*. (**B**) Multi-unit population data. Note the scale change on the x-axes between (A) and (B). Though, by chance, there turned out to be slightly greater initial selectivity at the swap position than the non-swap position, our reported effect was still strongly present even when post-hoc analysis was used to eliminate this initial selectivity difference (see Table S2 and Fig S8).

Supporting figure S4

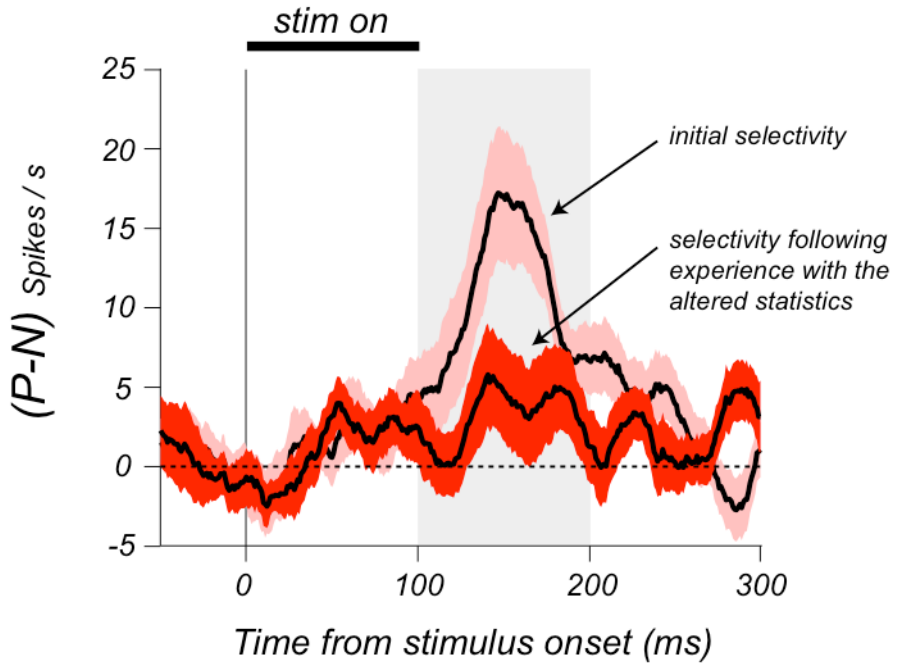

Fig. S4. The response time course of the IT selectivity (measured in the *Test Phase*, see Materials and methods) before and after at least one hour of experience in the altered visual world. The plot shows the averaged PSTH difference between object P and N. Colored area indicates the standard error of the mean. Only the neurons (n = 17) and multi-unit sites (n = 10) held for the longest exposure time are included in the plot. Each neuron's PSTH was computed by smoothing the response data with a Gaussian window (s.d. 10 ms). The responses are aligned at the onset of the stimulus. The black bar on the top indicates the duration of the stimulus. Note that the change in selectivity following experience was present even in the earliest part of the response (~100 ms). The same neurons showed no change for objects presented at the equally eccentric (non-swap) retinal position (time course not shown; see Figs. 2, 3).

Supporting figure S5

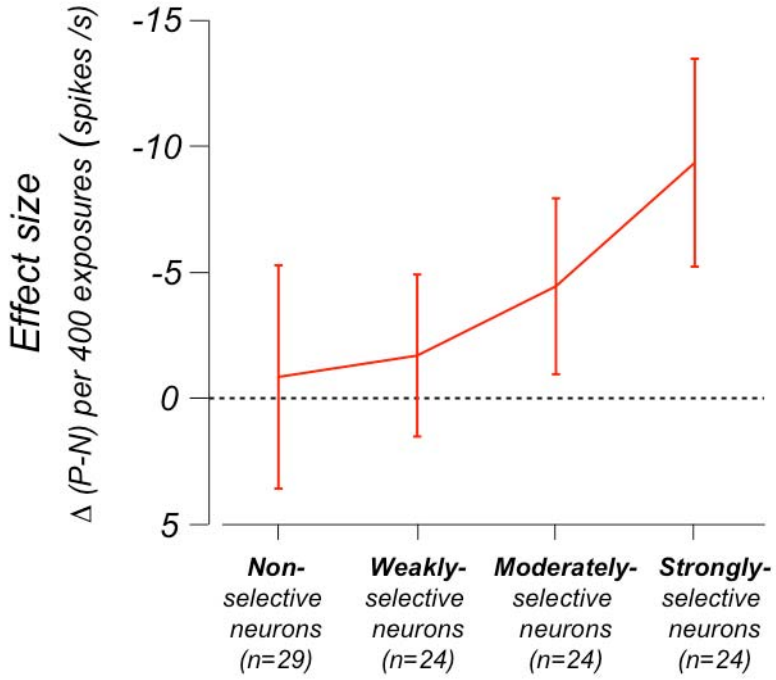

Fig. S5. Relationship between the magnitude of the learning effect and the IT neurons' object selectivity at the center of gaze. The abscissa shows neurons grouped by the amount of object selectivity at the center of gaze ("Non-selective neurons" are those with object selectivity (P-N) less than 1 spike/s; the remaining neurons were split into three even groups). The mean selectivity among the particular tested two objects (P and N) in the three groups was: 2, 5, and 15 spikes/s. The ordinate shows the mean experience-dependent effect size for the neurons in each group. Effect size was estimated for each neuron using regression analysis that leverages all the available data for each neuron (same as in Fig. 4C), so it reflects an unbiased estimate of effect size that is not confounded by any differences in total duration of exposure. There was no correlation between this effect size estimate and the duration of exposure ($r = 0.05$, $p = 0.62$). The plot shows the mean effect size in each group of neurons and s.e.m. When the same analysis was carried out at the non-swap position, the effect sizes were near zero for all four groups of neurons (not shown).

Supporting figure S6

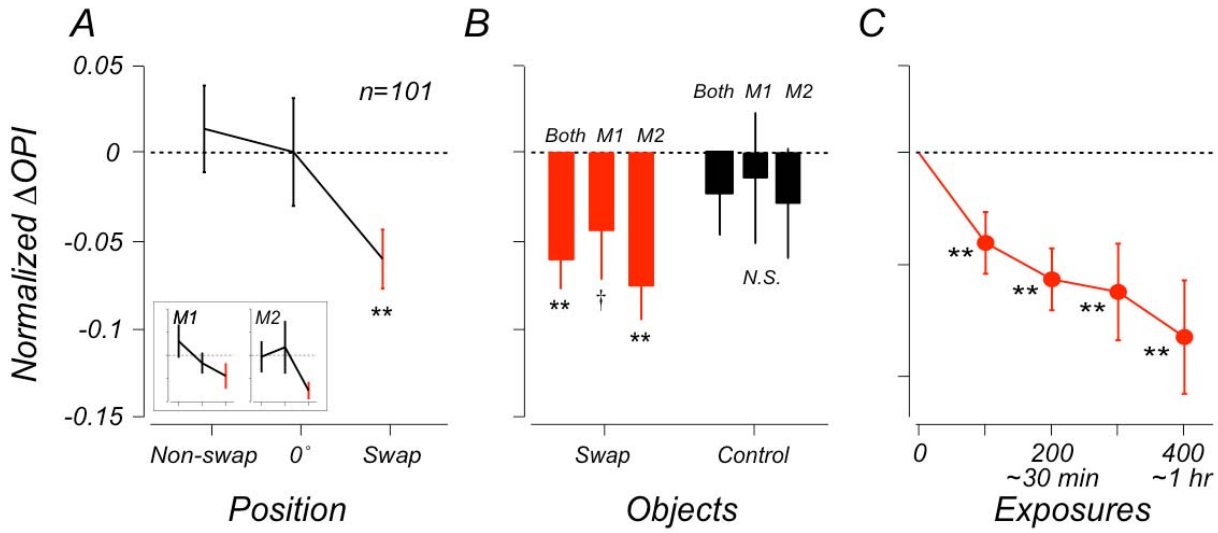

Fig. S6. Results in another selectivity metric. Here, results from all the neurons are re-plotted in the format of Fig. 3 but in normalized ΔOPI metric. (** significantly less than 0 at $p < 0.001$, one tailed t-test; N.S. $p > 0.05$; † approaching significance, $p = 0.058$).

Supporting figure S7

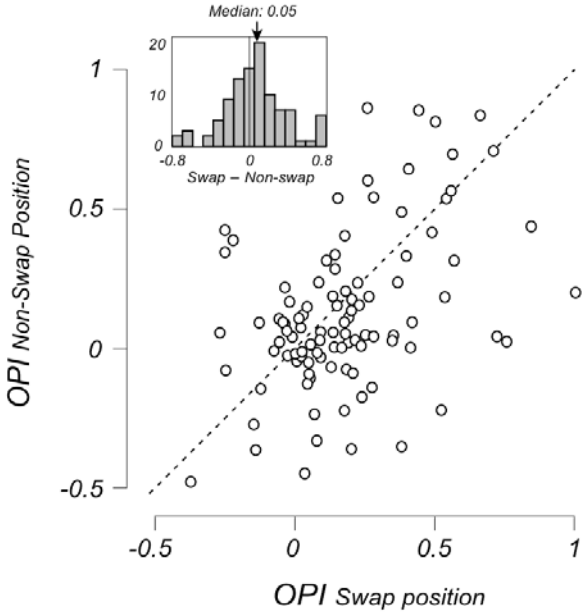

Fig. S7. Initial object selectivity (OPI) of all the neurons at the swap position and non-swap position. Because the object P and N are determined from the summed response across all positions using separate data, and IT neurons are not perfectly position-tolerant, the object selectivity at any given position (swap or non-swap) could have initially negative values. The inset shows the histogram of the object selectivity difference between the swap and non-swap positions. Though, by chance, there turned out to be slightly greater initial selectivity at the swap position than the non-swap position, our reported effect was still strongly present even when post-hoc analysis was used to eliminate this initial selectivity difference (see Table S2 and Fig S8). This plot also illustrates the broad distribution of selectivity in the full population, including some neurons with weak or negative selectivity (see Fig.S5 above).

Supporting figure S8

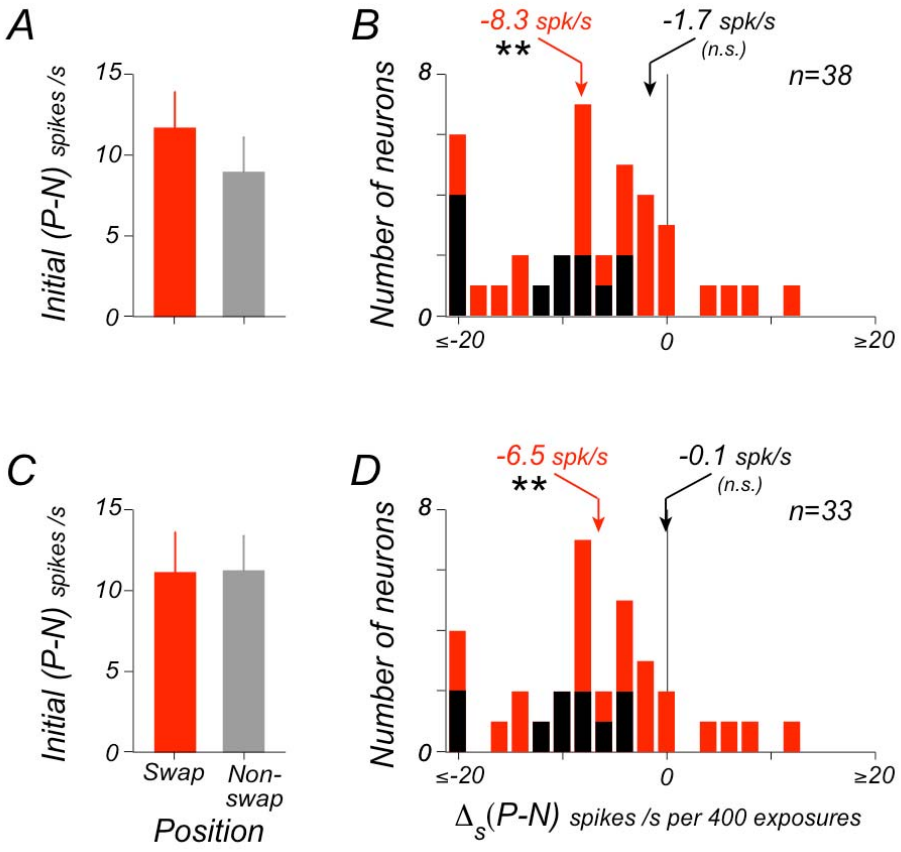

Fig. S8. Post-hoc selection to eliminate the initially greater selectivity at the swap position among the 38 highly object selective neurons/sites tested for at least 300 exposures (see main text). (**A**)(**B**) Data from the original set of 38 neurons. (**A**) mean selectivity at the swap and non-swap position before exposure. (**B**) is a re-plot of Fig 4C. Red arrow indicates the mean Δ_S(P-N). Black arrow indicates the mean Δ_S(P-N) from the non-swap position (individual neural data not shown). (** significantly less than 0 at $p < 0.001$, one tailed t-test; n.s. $p > 0.05$;) (**C**)(**D**) Re-make of (**A**) and (**B**) after neurons/sites with significantly greater selectivity at the swap position were discarded.

Supporting figure S9

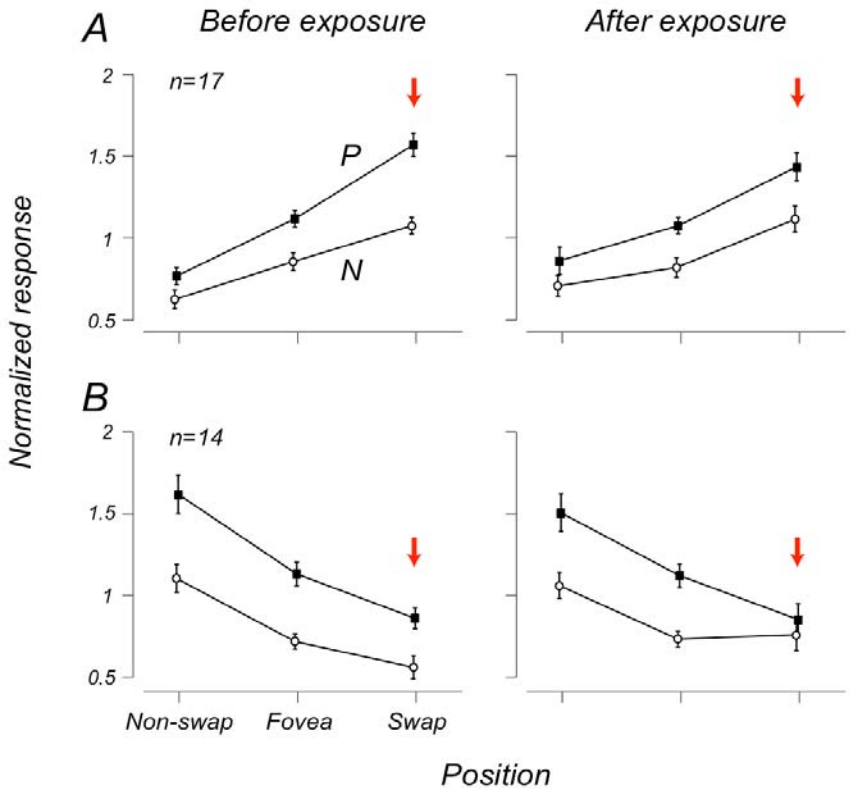

Fig. S9. Population response averages before and after exposure for those neurons preferring either the swap or non-swap position. Neurons were sorted by their receptive field profiles. Neurons in (**A**) were selected as those for which their maximum response (among either object) was evoked at the swap position and their minimum response at the non-swap position (n = 14; max and min taken among all three tested positions). Neurons in (**B**) were selected as those that had a maximum response at the non-swap position and minimum response at the swap position (n = 17). Neurons in (**A**) and (**B**) underwent, on average, ~200 exposures (~30 min). Each neuron's response was normalized to its averaged response to all objects at all positions before being combined in the group average. Error bars indicate the standard error of the mean.

Supporting figure S10

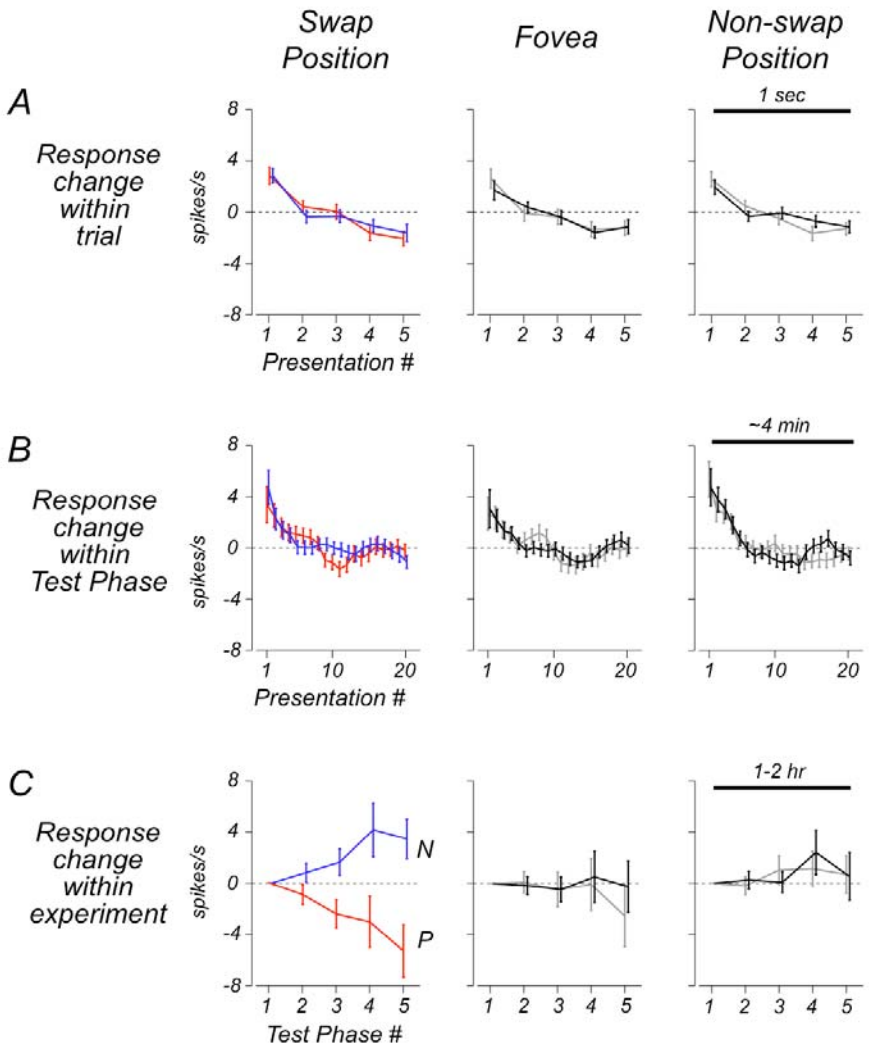

Fig. S10. Response changes across different time scales for the swap objects. (**A**) Population mean response changes within a trial (n=111, single-unit data and multi-unit data combined). For each neuron, the mean responses to each object at each position were subtracted before averaging. Responses were binned by the order in which the image (object at a position) appeared in the sequence of stimuli shown in the trial. (**B**) Population mean response changes within a *Test Phase*. For each neuron, the mean responses to each object at each position from the *Test Phases* were subtracted before averaging. Responses were binned by the order they appear in a *Test Phase* (20 - 30 repeats of each object at each position were tested during each *Test Phase*; see Materials and methods). These plots are smoothed with a sliding window (4 data point wide). (**C**) Population mean response changes across multiple *Test Phases (*the left plot in this row illustrates one view of our reported learning effect). For each neuron, the mean responses from the first *Test Phase* (pre-exposure) were subtracted before averaging. Red and gray traces show responses to object P; blue and black traces show responses to object N.

Supporting figure S11

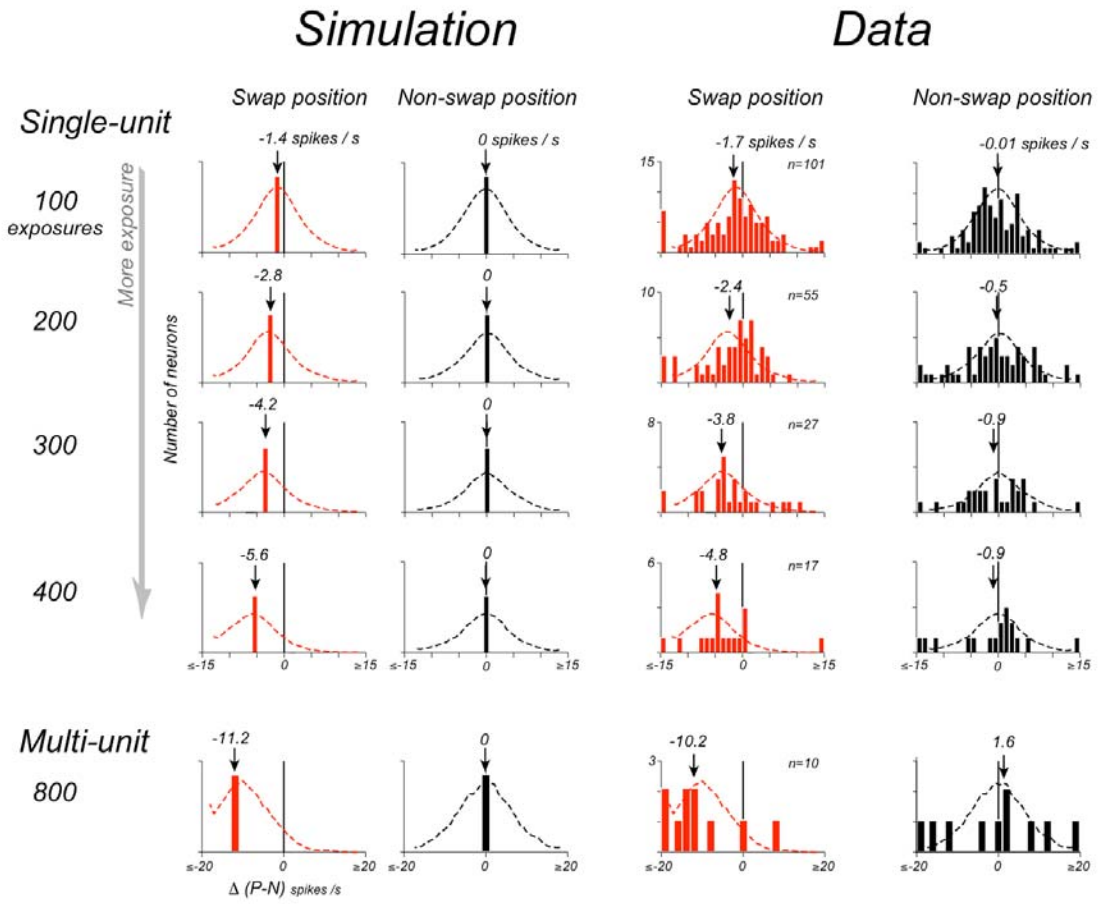

Fig. S11. Simulations to compare the expectations of Poisson spiking variability predictions with our experimental observed variation in object selectivity. The left panels show the average effect size (change in object selectivity) at each time point estimated from our data at the swap position (red bars and arrows, based on 5.6 spikes/s per 400 exposures, see Fig. 3C) and at the non-swap position (black bars and arrows, assuming no-change, see Fig. 2A). The smooth curves show the averaged histogram expected under the assumption of Poisson spiking statistics (using 100 Monte Carlo runs assuming: the same distribution of mean firing rates as that observed in the recorded population, the same number of response repetitions as that collected in our experiments: 30 for single-unit, 50 multi-units). The right panel shows the data from the recorded population. (The red histograms for the single-unit data is a re-plot of Fig. 2C). Arrows indicate the mean object selectivity changes observed in the data. The over-laid dash lines are the distributions generated from the simulations (left), simply re-plotted on top of the data. Note that the dashed curves are quite broad (the effect of Poisson spiking "noise") and are approximately matched to the empirical distributions (solid histograms).

Supporting figure S12

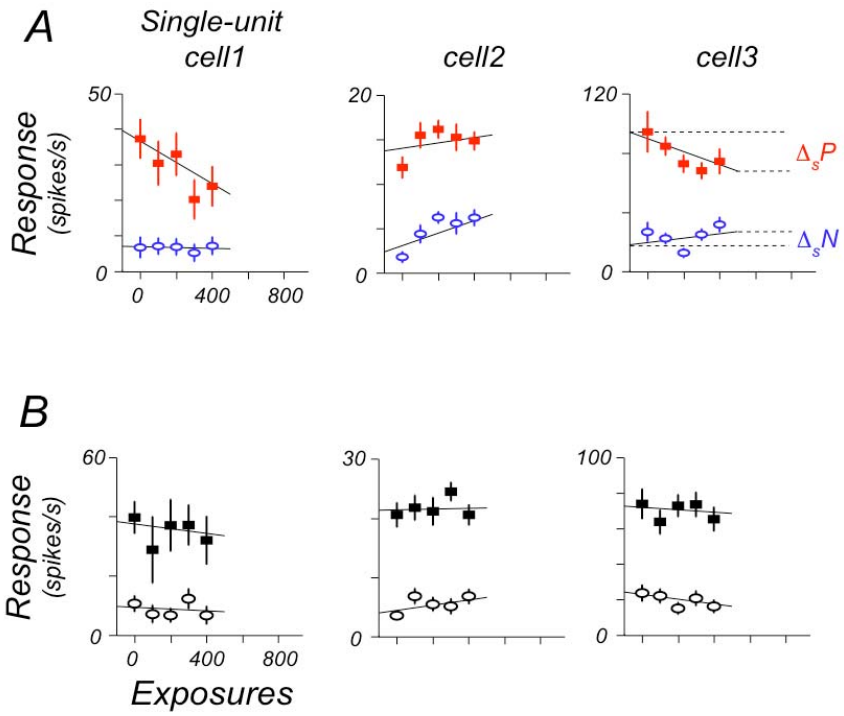

Fig. S12. Responses to objects P and N from example neurons in Fig. 4A. (**A**) Response data to object P and N at the swap position (This is a re-plot of the neurons in Fig. 4A). (**B**) Response data from the non-swap position for these neurons. The object P and N are determined from the summed response across all positions using separate data before exposure. In both panels, the solid lines are the best-fit linear regression.

Supporting table S1

Screen criteria based on responses at the center of gaze	Mean response rates under each screen (spikes/s)						Permutation Test for "position x exposure" interaction	t-Test swap vs. non-swap position
	Center of gaze		Swap position		Non-swap position			
	P	N	P	N	P	N		
Full population (no screen) n=101	20	14	21	16	20	16	*p = 0.007	*p = 0.005
Statistically selective (i.e. P>N at p<0.05) n=56	25	16	27	19	25	19	*p = 0.010	*p = 0.023
Statistically selective AND (P-N)>3 spikes/s n=48	29	18	29	20	27	20	*p = 0.016	*p = 0.041
Statistically selective AND (P-N)>5 spikes/s n=38	33	20	32	21	30	22	*p = 0.039	*p = 0.025

Table S1. Summary of key statistical tests on different subsets of center-of-gaze-selective neurons. Left table columns show the mean responses of all the neurons in each subset to objects P and N. The selectivity screens were done after the "P" and "N" labels were determined using separate data to avoid bias (that is, a positive response difference implies real selectivity for P over N, not selection bias). The P-N differences are greater at the swap position for all groups of neurons because a few most foveal selective neurons (3/38) had much greater selectivity at the swap position. The right columns show the outcome of the two key statistical analyses. These results are robust to removal of outlier points (Fig 2C top panel, left-most bar). Though the overall mean effect size per neuron is larger for more selective neurons (i.e. going from the top to the bottom of the table, see Fig. S5), the statistical significance level (p values) is slightly smaller (slightly larger p value) due to the drop in the number of neurons.

Supporting table S2

	Difference in (P-N) $_{\text{pre-exposure}}$ Swap – Non-swap (spikes/s)	Effect size (spikes/s)	
		Swap position	**Non-Swap position**
Full population in Fig. 2, 3 (n=101)	2.05	-5.6 *	0.9 (n.s.)
Matched (P-N) $_{\text{pre-exposure}}$ (n=84)	-0.01	-4.2 *	0.73 (n.s.)

	Difference in (P-N) $_{\text{pre-exposure}}$ Swap – Non-swap (spikes/s)	Effect size (spikes/s)	
		Swap position	**Non-Swap position**
Object-selective neurons/sites in Fig. 4C (n=38)	2.70	-8.3 **	-1.7 (n.s.)
Matched (P-N) $_{\text{pre-exposure}}$ (n=33)	-0.34	-6.5 **	-0.1 (n.s.)

Table S2. Summary of the key results after the initially greater selectivity at the swap position were adjusted for post-hoc. Effect size, $\Delta_S(P–N)$, was estimated for each neuron using regression analysis that included all the available data for each neuron (same as in Fig. 4C). $\Delta_S(P–N)$ was significantly different from 0 only at the swap position (* $p<0.05$; ** $p<0.001$; one tailed t-Test).

Supporting references and notes

1. J. J. DiCarlo, J. H. R. Maunsell, *Nat. Neurosci.* **3**, 814 (2000).
2. D. A. Robinson, *IEEE Transactions on Biomedical Engineering* **101**, 131 (1963).
3. K. Tanaka, *Cereb Cortex* **13**, 90 (2003).
4. G. Kreiman *et al.*, *Neuron* **49**, 433 (2006).
5. D. Zoccolan, M. Kouh, T. Poggio, J. J. DiCarlo, *J. Neurosci.* **27**, 12292 (2007).
6. G. C. Baylis, E. T. Rolls, C. M. Leonard, *J. Neurosci.* **7**, 330 (1987).
7. J. J. DiCarlo, J. H. R. Maunsell, *J. Neurophysiol.* **89**, 3264 (2003).
8. B. Efron, R. J. Tibshirani, *An Introduction to the Bootstrap.* (Chapman & Hall, 2003)
9. C. I. Baker, M. Behrmann, C. R. Olson, *Nat. Neurosci.* **5**, 1210 (2002).
10. N. Sigala, N. K. Logothetis, *Nature* **415**, 318 (2002).
11. H. Sawamura, G. A. Orban, R. Vogels, *Neuron* **49**, 307 (2006).
12. E. K. Miller, L. Li, R. Desimone, *Science* **254**, 1377 (1991).
13. S. Sobotka, J. L. Ringo, *Exp. Brain. Res.* **96**, 28 (1993).
14. C. G. Gross, P. H. Schiller, C. Wells, G. L. Gerstein, *J. Neurophysiol.* **30**, 833 (1967).
15. G. C. Baylis, E. T. Rolls, *Exp. Brain. Res.* **65**, 614 (1987).
16. D. J. Tolhurst, J. A. Movshon, A. F. Dean, *Vision Res.* **23**, 775 (1983).
17. M. N. Shadlen, W. T. Newsome, *J. Neurosc.* **18**, 3870 (1998).

Unsupervised Natural Experience Rapidly Alters Invariant Object Representation in Visual Cortex

Nuo Li, *et al.*

Science **321**, 1502 (2008);
DOI: 10.1126/science.1160028